The generalized Floquet-Bloch spectrum for periodic thermodiffusive layered materials

F. Fantoni[1*], L. Morini[2], A. Bacigalupo[3*], M. Paggi[4]

[1] *DICATAM, Università degli Studi di Brescia, via Branze 43, 25123, Brescia, Italy*
[2] *School of Engineering, Cardiff University, Cardiff, CF24 3AA, United Kingdom*
[3] *DICCA, Università degli Studi di Genova,via Montallegro 1, 16145 Genova, Italy*
[4] *IMT School for Advanced Studies Lucca, Piazza San Francesco 19, Lucca, 55100, Italy*

October 6, 2020

Abstract

The dynamic behaviour of periodic thermodiffusive multi-layered media excited by harmonic oscillations is studied. In the framework of linear thermodiffusive elasticity, periodic laminates, whose elementary cell is composed by an arbitrary number of layers, are considered. The generalized Floquet-Bloch conditions are imposed, and the universal dispersion relation of the composite is obtained by means of an approach based on the formal solution for a single layer together with the transfer matrix method. The eigenvalue problem associated with the dispersion equation is solved by means of an analytical procedure based on the symplecticity properties of the transfer matrix to which corresponds a palindromic characteristic polynomial, and the frequency band structure associated to wave propagating inside the medium are finally derived. The proposed approach is tested through illustrative examples where thermodiffusive multilayered structures of interest for renewable energy devices fabrication are analyzed. The effects of thermodiffusion coupling on both the propagation and attenuation of Bloch waves in these systems are investigated in detail.

Keywords: Periodic thermodiffusive laminates, Floquet-Bloch conditions, Transfer matrix, dispersion relation, complex spectra.

1 Introduction

In the last years, composite laminates subject to thermodiffusive phenomena have been largely used in the design and fabrication of renewable energy devices characterized by a multi-layered configuration, such as lithium-ion batteries (Ellis et al., 2012; Salvadori et al., 2014), solid oxide fuel cells (SOFCs) (Kakac et al., 2007; Colpan et al., 2008; Kim et al., 2009; Kuebler et al., 2010; Hasanov et al., 2011; Nakajo et al., 2012; Dev et al., 2014) and photovoltaic modules (PV) (Paggi et al., 2013). Several studies (Atkinson and Sun, 2007; Delette et al., 2013) have shown that, in real operative scenarios, performances in terms of power generation and energy conversion efficiency can be compromised because of the severe thermomechanical stress as well as intense particle flows to which components of such energy devices are subjected (Muramatsu et al., 2015). This can ultimately impact on their resistance to damage with resulting cracks formation and spreading. Consequently, modeling and predicting these phenomena is a crucial issue in order to ensure the successful manufacture of multi-layered renewable energy devices and to optimize their performances.

Energy devices of this kind are generally organized in stacks where more elements are separated by metallic interconnections (Molla et al., 2016). Due to their particular structure, these stacks constituted by series of connected energy devices can be modelled as periodic themodiffusive laminates which elementary cell, representing the single device, is composed by an arbitrary number of elasto-themodiffusive phases.

*Corresponding authors: Tel:+39 0303711330,
E-mail addresses: francesca.fantoni@unibs.it; andrea.bacigalupo@unige.it

Following this approach, an original asymptotic homogenization technique has been developed by Bacigalupo et al. (2014) and applied to the multi-field case by Bacigalupo et al. (2016a), Bacigalupo et al. (2016b), Fantoni et al. (2017, 2018), and Fantoni and Bacigalupo (2020) to study the static overall constitutive properties of composite structures of interest for energy devices applications. This method, based on the generalization of the rigorous procedure developed in Bakhvalov and Panasenko (1984), Smyshlyaev and Cherednichenko (2000), Bacigalupo et al. (2016b), Bacigalupo and Gambarotta (2014), provides exact closed-form expressions to estimate the overall elastic and themodiffusive tensors of multi-phase laminates avoiding the challenging computations required by standard numerical modelling of the heterogeneous structures (Bove and Ubertini, 2008; Richardson et al., 2012; Hajimolana et al., 2011). Nevertheless, an accurate description and understanding of dynamical phenomena in this type of laminate media and especially of the effects of the thermodiffusive coupling on the propagation and damping of mechanical waves and vibrations has not been addressed in details to the authors knowledge. Indeed, most of the work conducted on this topics have been performed adopting the generalized theories of thermoelasticity and thermodiffusion (Lord and Shulman, 1967; Sherief et al., 2004). These formulations provide thermal and diffusive relaxation times, and then the standard heat and mass conduction equations are transformed in hyperbolic type equations and both the temperature and the mass fields evolve in the medium in form of heat and diffusive waves having finite propagation speeds which interact with the mechanical waves. In contrast, the principal aim of this article is to study and estimate the impact of thermal and diffusive effects on the propagation of harmonic oscillations in two-dimensional thermodiffusive laminates of interest for energy applications. In our formulation, we assume that the elastic waves equation is coupled with the standard heat conduction and mass diffusion equations, which are of parabolic type, and are then associated with an imaginary part of the spectrum corresponding to damping phenomena. We implement the generalized Floquet-Bloch quasiperiodic conditions, and by means of a generalization of the transfer matrix method (Hawwa and Nayfeh, 1995), we derive a general expression for the characteristic equation valid for periodic thermodiffusive laminates which elementary cell is composed by an arbitrary number of phases. Symplecticity properties of the transfer matrix to which corresponds a palindromic characteristic polynomial are exploited in order to solve the eigenvalues problem associated with the characteristic equation, and this general procedure provides the frequency band structure (*complex spectra*) associated to wave propagating inside the medium. The potentialities of this technique are illustrated through illustrative examples where the propagation and damping of harmonic thermal and diffusive oscillations as well as of mechanical waves in bi-phase laminates of interest for SOFCs realization is addressed. The proposed original approach represents a powerful tool to study wave phenomena in multi-layered energy devices subject to thermodiffusion, and it can be easily applied to test and benchmark the results provided by both numerical and asymptotic local and nonlocal dynamic homogenization methods (Forest, 2002; Lew et al., 2004; Bigoni and Drugan, 2007; Scarpa et al., 2009; De Bellis and Addessi, 2011; Forest and Trinh, 2011; Bacca et al., 2013a,b; Wang et al., 2017; Fantoni et al., 2019; Kamotski and Smyshlyaev, 2019; Monchiet et al., 2020; Yvonnet et al., 2020). The paper is organized as follows: Section 2 summarizes governing equations for a linear thermodiffusive material and the wave-like expression of harmonic plane oscillations propagating inside the medium. Section 3 is dedicated to present the generalization of the transfer matrix method exploited to obtain, together with Floquet-Bloch conditions, complex spectra for thermodiffusive laminates. Representative examples are performed in Section 4, thus showing complex spectra obtained for bi-phase isotropic thermodiffusive laminates of interest for SOFCs fabrication in order to investigate the effects of thermodiffusive coupling upon propagation and damping properties of elastic waves traveling inside the composite. Finally, conclusions are addressed in Section 5.

2 Problem formulation

One considers a plane thermodiffusive laminate medium whose periodic cell is composed by an arbitrary number of layers n perfectly bonded at their interfaces and stacked along the x_2-axis (see figure 1). Each material point is identified by the position vector $\boldsymbol{x} = x_1\boldsymbol{e}_1 + x_2\boldsymbol{e}_2$ referred to a system of coordinates with origin at point O and orthogonal base $[\boldsymbol{e}_1, \boldsymbol{e}_2]$. The periodic cell $\mathcal{A} = (-\infty, +\infty) \times [0, L]$ is reported in figure 1-(b), and $L = \sum_{m=1}^{n} \ell_m$ where ℓ_m represents the thickness of each single layer. In this Section, governing equations valid for a single thermodiffusive layer are introduced, together with the formal wave-like solution describing harmonic plane oscillations propagating in the $x_1 - x_2$ plane.

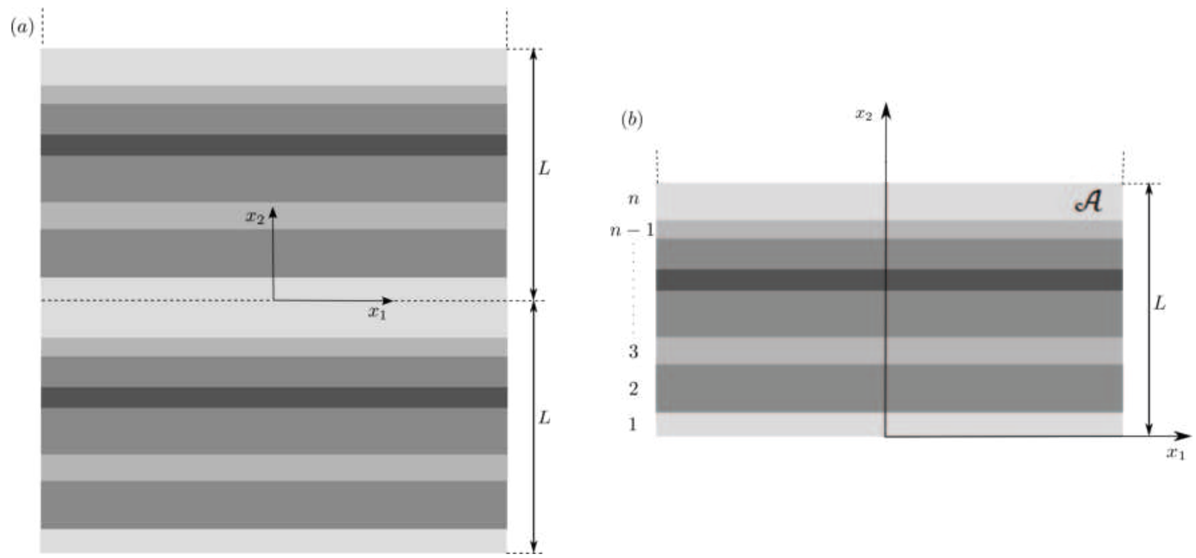

Figure 1: (a) Periodic thermodiffusive laminate; (b) Periodic cell $\mathcal{A}$ composed by n layers of arbitrary thickness.

2.1 Governing equations

Assuming that the constituent layers of the laminate are linear thermodiffusive elastic media, the three fields characterizing the behaviour of the thermodiffusive material are the displacement $\mathbf{u}(\mathbf{x},t) = u_i(\mathbf{x},t)\mathbf{e}_i$, the relative temperature $\theta(\mathbf{x},t) = T(\mathbf{x},t) - T_0$, with T_0 the temperature of the natural state, and the relative chemical potential $\eta(\mathbf{x},t) = P(\mathbf{x},t) - P_0$ with P_0 the chemical potential of the natural state. The stress tensor $\boldsymbol{\sigma}(\mathbf{x},t) = \sigma_{ij}(\mathbf{x},t)\mathbf{e}_i \otimes \mathbf{e}_j$, the heat flux vector $\mathbf{q}(\mathbf{x},t) = q_i(\mathbf{x},t)\mathbf{e}_i$, and the mass flux vector $\mathbf{j}(\mathbf{x},t) = j_i(\mathbf{x},t)\mathbf{e}_i$ are determined, respectively, through the following constitutive relations (Nowacki, 1974a,b,c)

$$\boldsymbol{\sigma}(\mathbf{x},t) = \mathfrak{C}\,\boldsymbol{\varepsilon}(\mathbf{x},t) - \boldsymbol{\alpha}\,\theta(\mathbf{x},t) - \boldsymbol{\beta}\,\eta(\mathbf{x},t), \tag{1}$$

$$\mathbf{q}(\mathbf{x},t) = -\mathbf{K}\,\nabla\theta(\mathbf{x},t), \tag{2}$$

$$\mathbf{j}(\mathbf{x},t) = -\mathbf{D}\,\nabla\eta(\mathbf{x},t), \tag{3}$$

with $\boldsymbol{\varepsilon}(\mathbf{x},t) = \mathrm{sym}\nabla\boldsymbol{u}(\mathbf{x},t)$ denoting the small strains tensor, $\mathfrak{C} = C_{ijkl}\mathbf{e}_i \otimes \mathbf{e}_j \otimes \mathbf{e}_k \otimes \mathbf{e}_l$ the fourth order elasticity tensor showing major and minor symmetries, $\boldsymbol{\alpha} = \alpha_{ij}\mathbf{e}_i \otimes \mathbf{e}_j$ the symmetric second order thermal dilatation tensor, $\boldsymbol{\beta} = \beta_{ij}\mathbf{e}_i \otimes \mathbf{e}_j$ the symmetric second order diffusive expansion tensor, $\mathbf{K} = K_{ij}\mathbf{e}_i \otimes \mathbf{e}_j$ the symmetric second order heat conduction tensor, and $\mathbf{D} = D_{ij}\mathbf{e}_i \otimes \mathbf{e}_j$ the symmetric second order mass diffusion tensor. For each constituent layer, the equations of motion, in the absence of body forces, are given by

$$\nabla \cdot \boldsymbol{\sigma}(\mathbf{x},t) = \rho\ddot{\mathbf{u}}(\mathbf{x},t), \tag{4}$$

whereas the energy and mass conservation, in the absence of source terms, lead, respectively, to the following equations (Nowacki, 1974a,b,c):

$$p\dot{\theta}(\mathbf{x},t) + \boldsymbol{\alpha}\dot{\boldsymbol{\varepsilon}}(\mathbf{x},t) + \psi\dot{\eta}(\mathbf{x},t) = -\nabla \cdot \boldsymbol{q}(\mathbf{x},t), \tag{5}$$

$$q\dot{\eta}(\mathbf{x},t) + \boldsymbol{\beta}\dot{\boldsymbol{\varepsilon}}(\mathbf{x},t) + \psi\dot{\theta}(\mathbf{x},t) = -\nabla \cdot \boldsymbol{j}(\mathbf{x},t), \tag{6}$$

Term ρ in equation (4) represents the mass density, p in equation (5) is a material constant depending upon the specific heat at constant strain and upon thermodiffusive effects, q in equation (6) is a material constant related to diffusive effects, and ψ is a material constant measuring thermodiffusive effects (Nowacki, 1974a,b,c). Substituting expressions (1), (2) and (3) into equations (4), (5) and (6), one obtains

$$\nabla \cdot (\mathfrak{C}\,\nabla\mathbf{u}(\mathbf{x},t)) - \nabla \cdot (\boldsymbol{\alpha}\,\theta(\mathbf{x},t)\,) - \nabla \cdot (\boldsymbol{\beta}\,\eta(\mathbf{x},t)\,) = \rho\,\ddot{\mathbf{u}}(\mathbf{x},t), \tag{7}$$

$$\nabla \cdot (\mathbf{K}\,\nabla\theta(\mathbf{x},t)) - \boldsymbol{\alpha}\,\nabla\dot{\boldsymbol{u}}(\mathbf{x},t) - \psi\,\dot{\eta}(\mathbf{x},t) = p\,\dot{\theta}(\mathbf{x},t), \tag{8}$$

$$\nabla \cdot (\mathbf{D}\,\nabla\eta(\mathbf{x},t)) - \boldsymbol{\beta}\,\nabla\dot{\boldsymbol{u}}(\mathbf{x},t) - \psi\,\dot{\theta}(\mathbf{x},t) = q\,\dot{\eta}(\mathbf{x},t). \tag{9}$$

Further in the text, propagation and damping of harmonic oscillations in thermodiffusive laminates are investigated, thus deriving a wave-like solution of the field equations in the form (7), (8) and (9).

2.2 Wave-like solution for a single layer

One considers harmonic plane oscillations propagating in the $x_1 - x_2$ plane, thus assuming that in any phase of the periodic thermodiffusive laminate the solution of the field equations (7), (8) and (9) takes the following form

$$\mathbf{v}(x_1, x_2, t) = (u_1 \; u_2 \; \theta \; \eta)^T = \mathbf{w}(x_2) \exp\left[i\left(\mathbf{k} \cdot \mathbf{x} - \omega t\right)\right], \tag{10}$$

where $\mathbf{k} = k_1 \boldsymbol{e}_1 + k_2 \boldsymbol{e}_2$, and $\mathbf{w}$ is the amplitudes vector

$$\mathbf{w}(x_2) = \left(\tilde{u}_1(x_2) \; \tilde{u}_2(x_2) \; \tilde{\theta}(x_2) \; \tilde{\eta}(x_2)\right)^T. \tag{11}$$

A generalized traction vector associated to the generalized displacements (10) can be defined as

$$\mathbf{s}(x_1, x_2, t) = (\sigma_{21} \; \sigma_{22} \; q_2 \; j_2)^T = \mathbf{t}(x_2) \exp\left[i\left(\mathbf{k} \cdot \mathbf{x} - \omega t\right)\right], \tag{12}$$

where $\mathbf{t}$ is given by

$$\mathbf{t}(x_2) = \left(\tilde{\sigma}_{21}(x_2) \;\; \tilde{\sigma}_{22}(x_2) \;\; \tilde{q}_2(x_2) \;\; \tilde{j}_2(x_2)\right)^T. \tag{13}$$

Substituting the solution expression (10) into field equations (7), (8) and (9), the following second order system of ODEs is derived

$$\mathbf{A}\,\mathbf{w}^{''} + \mathbf{B}\,\mathbf{w}^{'} + \mathbf{C}\,\mathbf{w} = \mathbf{0}, \tag{14}$$

where apex $'$ denotes the derivative with respect to the x_2-variable, and the 4×4 matrices $\mathbf{A}$, $\mathbf{B}$ and $\mathbf{C}$ are given by

$$\mathbf{A} = \begin{pmatrix} C_{1212} & 0 & 0 & 0 \\ 0 & C_{2222} & 0 & 0 \\ 0 & 0 & K_{22} & 0 \\ 0 & 0 & 0 & D_{22} \end{pmatrix},$$

$$\mathbf{B} = \begin{pmatrix} 2ik_2C_{1212} & ik_1(C_{1212}+C_{1122}) & 0 & 0 \\ ik_1(C_{1122}+C_{1212}) & 2ik_2C_{2222} & -\alpha_{22} & -\beta_{22} \\ 0 & i\omega\alpha_{22} & 2ik_2K_{22} & 0 \\ 0 & i\omega\beta_{22} & 0 & 2ik_2D_{22} \end{pmatrix},$$

$$\mathbf{C} = \begin{pmatrix} \begin{pmatrix} \rho\omega^2 \\ -k_1^2C_{1111} \\ -k_2^2C_{1212} \end{pmatrix} & -k_1k_2C_{1122} & -ik_1\alpha_{11} & -ik_1\beta_{11} \\ -k_1k_2C_{1212} & \begin{pmatrix} \rho\omega^2 \\ -k_1^2C_{1212} \\ -k_2^2C_{2222} \end{pmatrix} & -ik_2\alpha_{22} & -ik_2\beta_{22} \\ -\omega k_1\alpha_{11} & -\omega k_2\alpha_{22} & \begin{pmatrix} -k_1^2K_{11} \\ -k_2^2K_{22} \\ +i\omega p \end{pmatrix} & i\omega\psi \\ -\omega k_1\beta_{11} & -\omega k_2\beta_{22} & i\omega\psi & \begin{pmatrix} -k_1^2D_{11} \\ -k_2^2D_{22} \\ +i\omega q \end{pmatrix} \end{pmatrix}. \tag{15}$$

The general formal solution of system (14) is reported in details in the next Section for the most general case where thermodiffusive effects are coupled with mechanical displacement and stresses. Further in the paper, this formal solution, valid for a single layer of the laminate, is used together with the transfer matrix method in order to derive a general characteristic equation for studying dispersion and damping properties of the whole periodic cell associated to Floquet-Bloch conditions. Illustrative examples of applications are then proposed, considering the influence of coupling coefficients upon the global solution.

3 Transfer matrix method to determine the frequency band structure of a laminate composite

Introducing the eight-components vector $\mathbf{r} = (\mathbf{w}' \; \mathbf{w})^T$, one can easily transform the second order 4×4 system (14) in the following equivalent first order 8×8 system

$$\mathbf{M}\mathbf{r}' + \mathbf{N}\mathbf{r} = \mathbf{0}, \tag{16}$$

where $\mathbf{M}$ and $\mathbf{N}$ are 8×8 matrices

$$\mathbf{M} = \begin{pmatrix} \mathbf{A} & \mathbf{0} \\ \mathbf{0} & \mathbf{I} \end{pmatrix}, \quad \mathbf{N} = \begin{pmatrix} \mathbf{B} & \mathbf{C} \\ -\mathbf{I} & \mathbf{0} \end{pmatrix}. \tag{17}$$

General solution of first order ordinary differential system of equations (16) can be written as

$$\mathbf{r} = \exp\left[\mathbf{M}^{-1}\mathbf{N}x_2\right] \mathbf{c}, \tag{18}$$

where $\mathbf{c}$ is a vector of constants and the first $\exp[\cdot]$ denotes the matrix exponential. A possible procedure to compute matrix exponential is detailed in Appendix A. Denoting with $\mathbf{y}(x_1, x_2, t)$ a vector containing the components of solution vector $\mathbf{v}(x_1, x_2, t)$ of equation (10) and of the generalized traction vector $\mathbf{s}(x_1, x_2, t)$ of equation (12), it can be expressed in terms of $\mathbf{r}$ in the following way

$$\mathbf{y}(x_1, x_2, t) = \begin{pmatrix} \mathbf{v}(x_1, x_2, t) \\ \mathbf{s}(x_1, x_2, t) \end{pmatrix} = \exp\left[i(\mathbf{k} \cdot \mathbf{x} - \omega t)\right] \begin{pmatrix} \mathbf{0} & \mathbf{I} \\ \mathbf{R} & i\mathbf{R}k_2 + \mathbf{S} \end{pmatrix} \mathbf{r}, \tag{19}$$

where $\mathbf{I}$ is a 4×4 identity operator and matrices $\mathbf{R}$ and $\mathbf{S}$ are expressed as

$$\mathbf{R} = \begin{pmatrix} C_{1212} & 0 & 0 & 0 \\ 0 & C_{2222} & 0 & 0 \\ 0 & 0 & -K_{22} & 0 \\ 0 & 0 & 0 & -D_{22} \end{pmatrix}, \quad \mathbf{S} = \begin{pmatrix} 0 & 0 & 0 & 0 \\ 0 & 0 & -\alpha_{22} & -\beta_{22} \\ 0 & 0 & 0 & 0 \\ 0 & 0 & 0 & 0 \end{pmatrix}. \tag{20}$$

Plugging solution (18) into (19) one obtains

$$\mathbf{y}(x_1, x_2, t) = \begin{pmatrix} \mathbf{0} & \mathbf{I} \\ \mathbf{R} & i\mathbf{R}k_2 + \mathbf{S} \end{pmatrix} \exp\left[-\mathbf{M}^{-1}\mathbf{N}x_2\right] \mathbf{c} \exp\left[i(\mathbf{k} \cdot \mathbf{x} - \omega t)\right]. \tag{21}$$

If the single m^{th} layer belonging to the periodic cell shown in figure 1 has thickness ℓ_m, referring to a local coordinate system as the one depicted in figure 2, such as along the x_2-axis the layer extends in the range $-\ell_m/2 \leq x_2 \leq \ell_m/2$, one can define the generalized vector $\mathbf{y}$ containing displacement components, relative temperature, relative chemical potential, tractions, heat and mass fluxes at the upper and lower boundary of the layer as

$$\mathbf{y}_m^+ = \mathbf{y}_m(x_1, x_2 = \ell_m/2, t) = \begin{pmatrix} \mathbf{0} & \mathbf{I} \\ \mathbf{R} & i\mathbf{R}k_2 + \mathbf{S} \end{pmatrix} \exp\left[-\mathbf{M}^{-1}\mathbf{N}\ell_m/2\right] \mathbf{c} \exp\left[i(k_1 x_1 + k_2 \ell_m/2 - \omega t)\right], \tag{22}$$

$$\mathbf{y}_m^- = \mathbf{y}_m(x_1, x_2 = -\ell_m/2, t) = \begin{pmatrix} \mathbf{0} & \mathbf{I} \\ \mathbf{R} & i\mathbf{R}k_2 + \mathbf{S} \end{pmatrix} \exp\left[\mathbf{M}^{-1}\mathbf{N}\ell_m/2\right] \mathbf{c} \exp\left[i(k_1 x_1 - k_2 \ell_m/2 - \omega t)\right]. \tag{23}$$

From equation (23) constants vector $\mathbf{c}$ gains the form

$$\mathbf{c} = \exp\left[-\mathbf{M}^{-1}\mathbf{N}\ell_m/2\right] \begin{pmatrix} \mathbf{0} & \mathbf{I} \\ \mathbf{R} & i\mathbf{R}k_2 + \mathbf{S} \end{pmatrix}^{-1} \mathbf{y}_m^- \exp\left[i(k_1 x_1 - k_2 \ell_m/2 - \omega t)\right]. \tag{24}$$

Substitution of expression (24) into (22) leads to express $\mathbf{y}_m^+$ in terms of $\mathbf{y}_m^-$ as

$$\mathbf{y}_m^+ = \begin{pmatrix} \mathbf{0} & \mathbf{I} \\ \mathbf{R} & i\mathbf{R}k_2 + \mathbf{S} \end{pmatrix} \exp\left[-\mathbf{M}^{-1}\mathbf{N}\ell_m\right] \begin{pmatrix} \mathbf{0} & \mathbf{I} \\ \mathbf{R} & i\mathbf{R}k_2 + \mathbf{S} \end{pmatrix}^{-1} \exp\left[ik_2\ell_m\right] \mathbf{y}_m^- = \mathbf{T_m}\, \mathbf{y}_m^-, \tag{25}$$

where $\mathbf{T}_m$ is the frequency-dependent transfer matrix of the m^{th} thermodiffusive elastic layer (Gupta, 1970; Faulkner and Hong, 1985). Since relation (25) is valid for each single layer forming the periodic cell and since it is assumed that the layers are perfectly bonded, so that continuity condition

$$\mathbf{y}_m^+ = \mathbf{y}_{m+1}^- \tag{26}$$

must be satisfied at the interface between two subsequent layers m and $m+1$ (see figure 2), the following equation can be easily derived relating generalized vector at the upper boundary of the last n^{th} layer $\mathbf{y}_n^+$ to the generalized vector at the lower boundary of the first layer $\mathbf{y}_1^-$

$$\mathbf{y}_n^+ = \mathbf{T}_{(1,n)}\,\mathbf{y}_1^-, \tag{27}$$

where $\mathbf{T}_{(1,n)} = \prod_{i=0}^{n-1} \mathbf{T}_{n-i}$ is the frequency-dependent transfer matrix of the entire periodic cell.

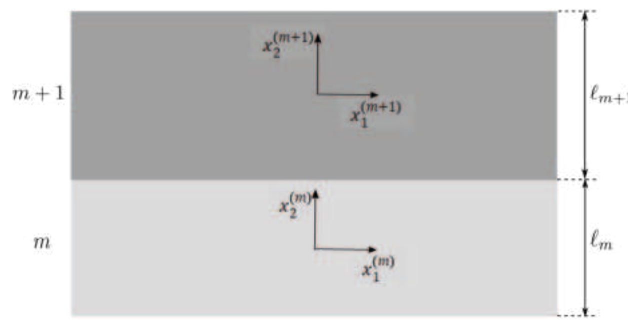

Figure 2: Two subsequent layers of arbitrary thickness belonging to the periodic cell. Local systems of coordinates used for deriving the transfer matrix of each layer are reported.

In order to investigate the propagation and damping of plane oscillations in a periodic laminates with unit cell composed by n layers stacked along the x_2-axis, the following Floquet-Bloch boundary condition (Floquet, 1883; Bloch, 1929; Brillouin, 1953; Mead, 1973; Langley, 1993) can be imposed

$$\mathbf{y}_n^+ = \exp\left[ik_2 L\right]\mathbf{y}_1^- \tag{28}$$

where, due to the geometry of the system (see figure 1), the periodicity direction is assumed to be along the x_2-axis and $L = \sum_{m=1}^{n} \ell_m$ is the extent of the whole periodic cell along that direction. Substituting (28) into (27) one obtains the following standard eigenvalue problem

$$\left(\mathbf{T}_{(1,n)} - \lambda\mathbf{I}\right)\mathbf{y}_1^- = \mathbf{0}, \tag{29}$$

where $\lambda = \exp\left[ik_2 L\right]$ is called Floquet multiplier and $\mathbf{I}$ represents an 8×8 identity operator. The system (29) admits non-trivial solution when the following characteristic equation is satisfied

$$\mathcal{D}(\mathbf{k},\omega) = \mathrm{Det}\left(\mathbf{T}_{(1,n)} - \lambda\mathbf{I}\right) = 0. \tag{30}$$

Equation (30) is the dispersion relation of plane oscillations in periodic thermodiffusive laminates where the elementary cell is composed by an arbitrary number of layers n. Furthermore, transfer matrix $\mathbf{T}_{(1,n)}$ results to be a symplectic matrix having a unitary determinant. In the most general case, both the wave vector $\mathbf{k}$ and the angular frequency ω, to which characteristic equation $\mathcal{D}$ depends, can be complex, namely $\mathbf{k} = (k_{1r} + i\,k_{1i})\mathbf{e}_1 + (k_{2r} + i\,k_{2i})\mathbf{e}_2$ and $\omega = \omega_r + i\,\omega_i$. In this case, wave vector $\mathbf{k}$ can be written in the form

$$\mathbf{k} = \mathbf{k}_r + i\mathbf{k_i} = k_r\,\mathbf{n}_r + i\,k_i\,\mathbf{n}_i, \tag{31}$$

where $\mathbf{k}_r$ represents the real wave vector having magnitude k_r and direction $\mathbf{n}_r \in \mathbb{R}^2$, and $\mathbf{k}_i$ is the attenuation vector with magnitude k_i and direction $\mathbf{n}_i \in \mathbb{R}^2$. A plane wave can be defined as homogeneous when the direction of normals to planes of constant phase $\mathbf{n}_r$ coincides with the one of normals to planes of constant amplitude $\mathbf{n}_i$, namely when $\mathbf{n}_r \times \mathbf{n}_i = \mathbf{0}$ (Carcione, 2007). Denoting with $\mathbf{n}$ such a direction one has

$$\mathbf{k} = (k_r + i\,k_i)\,\mathbf{n} = \kappa\,\mathbf{n}, \tag{32}$$

with κ the complex wave number. Furthermore, being $\mathbf{k}_r/k_r = \mathbf{k}_i/k_i$, for an homogeneous wave one obtains the following relation among the real and imaginary parts of k_1 and k_2

$$k_{1r}\, k_{2i} = k_{2r}\, k_{1i}. \tag{33}$$

When $\mathbf{k} \in \mathbb{C}^2$ and $\omega \in \mathbb{C}$, frequency spectrum is determined from the intersection of two hypersurfaces immersed in a space in $\mathbb{R}^6$, representing respectively the vanishing of the real and imaginary part of characteristic equation (30), namely

$$\begin{cases} \mathrm{Re}\left(\mathcal{D}\left(k_{1r}, k_{1i}, k_{2r}, k_{2i}, \omega_r, \omega_i\right)\right)) = 0 \\ \mathrm{Im}\left(\mathcal{D}\left(k_{1r}, k_{1i}, k_{2r}, k_{2i}, \omega_r, \omega_i\right)\right) = 0 \end{cases}. \tag{34}$$

In order to investigate spatial damping for the material at hand, the wave vector $\mathbf{k}$ is considered as complex ($k_\alpha = k_{\alpha r} + i\, k_{\alpha i}$ with $\alpha = 1, 2$) and the angular frequency ω as real (Caviglia and Morro, 1992). In the particular case where the value of one component k_α is fixed ($\alpha = 1$ or $\alpha = 2$), frequency spectrum is obtained through the intersection of two surfaces in $\mathbb{R}^3$, namely the plane $\{k_{\beta r}, k_{\beta i}, \omega\}$, with $\beta \neq \alpha$, as

$$\begin{cases} \mathrm{Re}(\mathcal{D}(k_{\beta r}, k_{\beta i}, \omega)) = 0 \\ \mathrm{Im}(\mathcal{D}(k_{\beta r}, k_{\beta i}, \omega)) = 0 \end{cases}, \tag{35}$$

and, if fixing k_α equation (33) results satisfied, the plane wave is homogeneous. By fixing, for example, component k_1 of complex wave vector $\mathbf{k}$, a procedure for obtaining material frequency band structure that is alternative to (35) is to directly solve linear eigenvalue problem (29), where the Floquet multiplier λ is the eigenvalue and $\mathbf{y}_1^-$ is the eigenvector. In this situation, in fact, it is possible to prove that transfer matrix $\mathbf{T}_{(1,n)}$ results to be independent upon k_2 and characteristic equation (30) reduces to the 8^{th}-degree associated polynomial. In this case, being the wave number related to the Floquet multiplier by relation $k_2 = \ln(\lambda)/(i\, L)$, its real and imaginary parts are expressed in terms of $\lambda = \lambda_r + i\, \lambda_i$ as

$$k_{2r} = \frac{\mathrm{Arg}(\lambda_r + i\, \lambda_i)}{L}, \qquad k_{2i} = -\frac{1}{2}\frac{\ln(\lambda_r^2 + \lambda_i^2)}{L}, \tag{36}$$

where symbol $\mathrm{Arg}(\cdot)$ denotes the argument of a complex number. As expected, $k_{2r}L$ is a function whose values belong to the first, dimensionless, Brillouin zone $(-\pi, \pi]$. Figure 3 shows the behaviour of dimensionless wave numbers $k_{2r}^* = k_{2r}L$ and $k_{2i}^* = k_{2i}L$ in terms of the real and imaginary parts of Floquet multiplier λ. As depicted in figure 3-(a), k_{2r}^* shows a branch cut discontinuity in the complex λ plane running from $-\infty$ to 0. Moreover, since $\mathbf{T}_{(1,n)}$ is a symplectic matrix, if λ_k is the k^{th} eigenvalue for characteristic equation (30), also

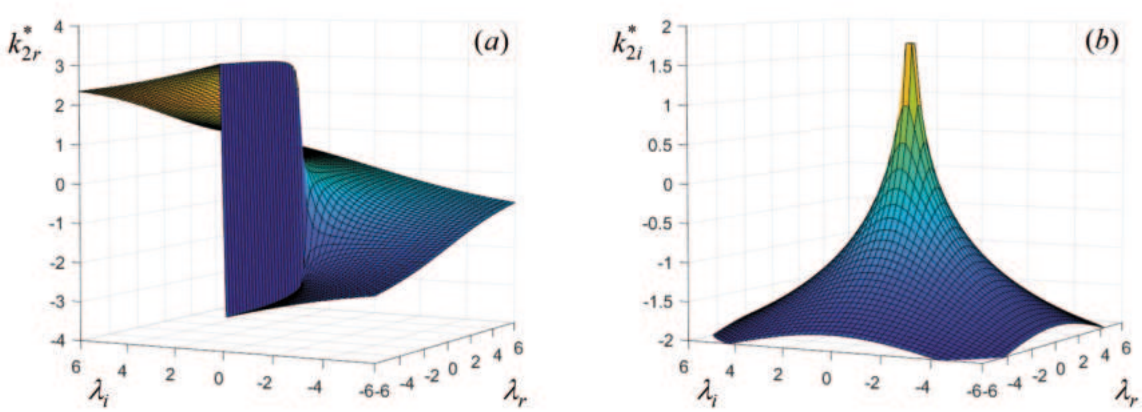

Figure 3: *(a) dimensionless wave number k_{2r}^* as a function of the real and imaginary parts of the Floquet multiplier λ. (b) dimensionless wave number k_{2i}^* as a function of the real and imaginary parts of the Floquet multiplier λ*

$1/\lambda_k$ is an eigenvalue. Such eigenvalues, in fact, are the roots of a palindromic characteristic polynomial, which is characterized by a reduced number of invariants (Hennig and Tsironis, 1999; Romeo and Luongo, 2002; Bronski and Rapti, 2005; Xiao et al., 2013; Carta and Brun, 2015; Carta et al., 2016). A procedure to compute the invariants of such characteristic polynomial is detailed in Appendix B. When component k_2 of $\mathbf{k}$ is fixed, in order to study wave propagation in the $\mathbf{e}_1$ direction, one could exploit the formal solution outlined in Appendix C, which allows expressing transfer matrix $\mathbf{T}_m$ of the single m^{th} layer as a power series of wave number k_1. In this way, by combining transfer matrices of all the n layers constituting the periodic cell, one obtains the transfer matrix of the entire cell $\mathbf{T}_{(1,n)}$ as a power series of k_1. Truncating this last at a proper order, it is possible to obtain an approximation of the eigenvalue problem (30) showing a polynomial dependence upon k_1, which can be used to investigate propagation of plane waves in the $\mathbf{e}_1$ direction. Temporal damping is studied by considering the angular frequency ω in (30) as complex ($\omega = \omega_r + i\,\omega_i$) and wave vector $\mathbf{k}$ as real (Carcione, 2007). In this case, once a component of $\mathbf{k}$ is fixed (k_α with $\alpha = 1$ or 2), frequency spectrum is obtained by means of the intersection between two surfaces in $\mathbb{R}^3$, namely the plane $\{k_\beta, \omega_r, \omega_i\}$, with $\beta \neq \alpha$. Such surfaces represent the vanishing of the real and imaginary parts of implicit function $\mathcal{D}$, namely

$$\begin{cases} \mathrm{Re}(\mathcal{D}(k_\beta, \omega_r, \omega_i)) = 0 \\ \mathrm{Im}(\mathcal{D}(k_\beta, \omega_r, \omega_i)) = 0 \end{cases} . \tag{37}$$

Analogously to what done for spatial damping, Appendix D describes a formal procedure to express transfer matrix of a single layer as a power series of angular frequency ω. Following the same path of reasoning as before, transfer matrix of the entire periodic cell can thus be truncated at a proper order of ω in order to obtain a useful approximation of the eigenvalue problem (30) with a polynomial dependence upon ω with the aim of investigating temporal damping for the material at hand.

4 Illustrative examples

Solution of the general characteristic equation (30) is performed in the followings for thermodiffusive multi-layered systems of interest for engineering and technology applications. In particular, the behaviour of a thermodiffusive bi-layered composite which can be used in the fabrication of solid oxide fuel cells (SOFCs) (Bacigalupo et al., 2014, 2016b; Fantoni and Bacigalupo, 2020), is explored. Propagation and damping of harmonic oscillations is examined inside the system by solving the linear eigenvalue problem (29), where the Floquet multiplier λ represents the eigenvalue. Referring to coordinate system represented in figure 2, for a fixed value of k_1, the behaviour of real and imaginary parts of k_2, related, respectively, to the propagating part and to the spatial attenuation of the wave (spatial damping), is investigated with respect to the real independent parameter ω. By means of a parametric analysis, the effects of the coupling between thermal, diffusive and mechanical fields on the dispersion and damping curves as well as their physical implications are discussed in details.

4.1 Dispersion and damping in bi-phase thermodiffusive layered media of interest for SOFC devices fabrication

One considers a periodic bi-phase laminate composed by materials of interest for solid oxide fuel cells fabrication, similar to those introduced in Bacigalupo et al. 2016a. Phase 1, representing the SOFC's ceramic electrolyte, is assumed to be constituted by Yttria-stabilized zirconia (YSZ), whereas phase 2, representing an electrode (cathode or anode), is assumed to be made by a Nichel-based ceramic-metallic composite material (see for example Zhu and Deevi 2003, Brandon and Brett 2006). Propagation of plane harmonic Bloch waves which can be modelled using expression (10) is explored. In the calculations, both layers are considered to have the same thickness $\ell_1 = \ell_2 = 1$ mm. Assuming a plane strain condition and isotropic phases constitutive equations (1)-(3) simplifies into

$$\boldsymbol{\sigma}(\mathbf{x}, t) = 2G\boldsymbol{\varepsilon}(\mathbf{x}, t) + \left(\frac{2\nu G}{1-2\nu} \mathrm{tr}\left[\boldsymbol{\varepsilon}(\mathbf{x}, t) \right] - \alpha\theta(\mathbf{x}, t) - \beta\eta(\mathbf{x}, t) \right) \mathbf{I}, \tag{38}$$

$$\mathbf{q}(\mathbf{x}, t) = -K\nabla\theta(\mathbf{x}, t), \tag{39}$$

$$\mathbf{j}(\mathbf{x}, t) = -D\nabla\eta(\mathbf{x}, t), \tag{40}$$

with shear modulus G expressed in terms of Young's modulus E and Poisson ration ν as $G = E/(2(1+\nu))$, $\alpha = 2G(1+\nu)\alpha_t/(1-2\nu)$ being α_t the coefficient of linear thermal dilation, $\beta = 2G(1+\nu)\beta_t/(1-2\nu)$

being β_t the coefficient of linear diffusion dilation, thermal conductivity constant K, and mass diffusivity constant D. For the phase 1 (YSZ-electrolyte), the values of the Young's modulus, Poisson's ratio and mass density are assumed to be respectively $E_1 = 155$ GPa, $\nu_1 = 0.3$ and $\rho_1 = 5532$ kg/m^3, whereas for the phase 2 (Ni-based composite) they are $E_2 = 50$ GPa, $\nu_2 = 0.25$ and $\rho_2 = 6670$ kg/m^3 (see Johnson and Qu 2008, Anandakumar et al. 2010 and Nakajo et al. 2012). Concerning the thermal properties of the layers, the thermal conductivities of the phases are $K_{t1} = 2.64$ W/mK and $K_{t2} = 9.96$ W/mK, the specific heats $C_1 = 400$ J/kgK and $C_2 = 440$ J/kgK and the temperature of the natural state is assumed to be $T_0 = 293.15$K. The normalized thermal conductivity and the thermodiffusive coefficient p_i introduced in the governing equations (7)-(9) are given, respectively, by $K_i = K_{ti}/T_0$ and $p_i = \rho_i C_i/T_0, \quad i = 1, 2$. Coefficients of linear thermal dilatation are given by $\alpha_{t1} = 2.2205 \cdot 10^{-6}\, 1/K$ and $\alpha_{t2} = 3.8858 \cdot 10^{-6}\, 1/K$, while coefficients of linear diffusion dilatation β_{ti} $(i = 1, 2)$ are assumed to have a value equal to 1/10 of the correspondent α_{ti}. Regarding the diffusive properties of the two layers, the ratio between the diffusion coefficient D_i and the thermodiffusive coefficient q_i used in equation (9) are assumed to be equal to $D_1/q_1 = 0.9 \cdot 10^{-5}$m^2/s and $D_2/q_2 = 0.73 \cdot 10^{-5}$m^2/s, with the value of q_i equal to 1/10 of the respective p_i $(i = 1, 2)$. Finally, thermodiffusive coupling coefficients ψ_i are taken with a value equal to 1/3 of the correspondent p_i.

For each phase matrices $\mathbf{A}, \mathbf{B}$, and $\mathbf{C}$ introduced in equation (14) assume the form

$$
\begin{aligned}
\boldsymbol{A} &= \begin{pmatrix} G & 0 & 0 & 0 \\ 0 & \dfrac{2G(1-\nu)}{1-2\nu} & 0 & 0 \\ 0 & 0 & K & 0 \\ 0 & 0 & 0 & D \end{pmatrix}, \\
\boldsymbol{B} &= \begin{pmatrix} 2ik_2G & \dfrac{ik_1G}{1-2\nu} & 0 & 0 \\ \dfrac{ik_1G}{1-2\nu} & \dfrac{4ik_2G(1-\nu)}{1-2\nu} & -\alpha & -\beta \\ 0 & i\omega\alpha & 2ik_2K & 0 \\ 0 & i\omega\beta & 0 & 2ik_2D \end{pmatrix}, \\
\boldsymbol{C} &= \begin{pmatrix} \left(\begin{matrix} \rho\omega^2 \\ -\dfrac{2k_1^2G(1-\nu)}{1-2\nu} \\ -Gk_2^2 \end{matrix}\right) & -\dfrac{k_1k_2G}{1-2\nu} & -ik_1\alpha & -ik_1\beta \\ -\dfrac{k_1k_2G}{1-2\nu} & \left(\begin{matrix} \rho\omega^2 \\ -k_1^2G \\ -\dfrac{2k_2^2G(1-\nu)}{1-2\nu} \end{matrix}\right) & -ik_2\alpha & -ik_2\beta \\ -\omega k_1\alpha & -\omega k_2\alpha & \left(\begin{matrix} -(k_1^2+k_2^2)K \\ +i\omega p \end{matrix}\right) & i\omega\psi \\ -\omega k_1\beta & -\omega k_2\beta & i\omega\psi & \left(\begin{matrix} -(k_1^2+k_2^2)D \\ +i\omega q \end{matrix}\right) \end{pmatrix}.
\end{aligned}
\tag{41}
$$

Figure 4 represents complex frequency spectrum obtained by solving standard eigenvalue problem (29) in the direction perpendicular to the material layering ($k_1 = 0$). In this case the plane wave propagating inside the material results to be homogeneous since $\mathbf{n}_r \equiv \mathbf{n}_i$ in equation (31). Complex-valued wave number k_2 has been determined for discrete values of the real-valued frequency ω in a selected range, spanning from 0 to $2 \cdot 10^7$. Figure 4-(a) plots the real and imaginary parts of wave number k_2, related to the complex-valued eigenvalue λ through equations (36), in terms of ω. In particular, real and imaginary parts of dimensionless wave number $k_2^* = k_2 L$ are plotted in terms of the real dimensionless frequency $\omega^* = \omega/\omega_{ref}$, being $\omega_{ref} = 1\,rad/s$ a reference frequency. MATLAB® enhanced with the Advanpix Multiprecision Toolbox has been exploited as a tool for computing transfer matrix $\mathbf{T}_{(1,n)}$ of the periodic cell and solving linear eigenvalue problem (29). The above mentioned toolbox allows computing using an arbitrary precision that, with respect to the usual double one, revealed to be an essential feature in order to obtain a unitary determinant for the symplectic matrix $\mathbf{T}_{(1,n)}$ and, consequently, to compute the right eigenvalues. Light blue curves of figure 4 represent the translation of the spectrum along the k_{2r}^* axis in order to emphasize the periodicity of the curves along

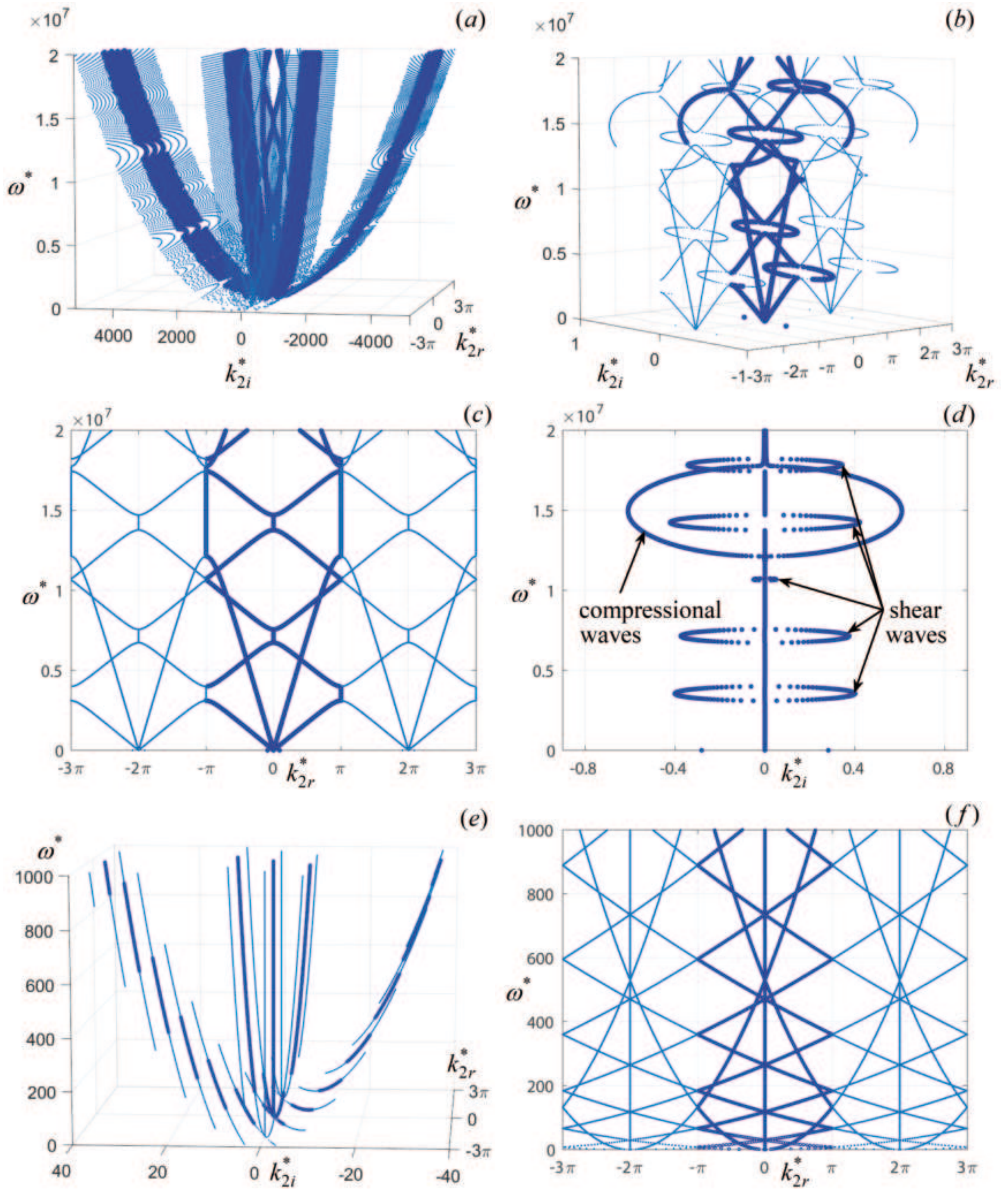

Figure 4: Complex frequency spectrum obtained for $k_1 = 0$. (a)3D view; (b) zoomed 3D view for $-1 \leq k_{2i}^* \leq 1$; (c) plane $k_{2r}^* - \omega^*$ for $-1 \leq k_{2i}^* \leq 1$; (d) plane $k_{2i}^* - \omega^*$ for $-1 \leq k_{2i}^* \leq 1$; (e) 3D view for $0 \leq \omega^* \leq 10^3$ and for $-40 \leq k_{2i}^* \leq 40$; (f) plane $k_{2r}^* - \omega^*$ for $0 \leq \omega^* \leq 10^3$.

this axis. Figure 4-(b) is a zoom of figure 4-(a) considering $-1 \leq k_{2i}^* \leq 1$, thus showing propagation branches related to the presence of hyperbolic equation (7) in the governing field equations set. Figures 4-(c) and 4-(d) are the two-dimensional representation of 4-(b) displaying, respectively, the planes $k_{2r}^* - \omega^*$ and $k_{2i}^* - \omega^*$.

They show, respectively, the structure of pass bands with real-valued wave number k_2^* corresponding to propagating waves, and the structure of band gaps with imaginary wave number k_2^*, which describes spatial wave attenuation due to material damping. Figure 4-(d) clearly plots the opening of different band gaps, related to both compressional and shear mechanical waves, where the second ones result to be uncoupled from thermal and diffusive fields being components α_{12} and β_{12} of constitutive tensors $\boldsymbol{\alpha}$ and $\boldsymbol{\beta}$, respectively, equal to zero for both phases of the unit cell. Figure 4-(e) is a zoomed view of figure 4-(a) with $0 \leq \omega^* \leq 10^3$ detailing the behaviour of damping branches due to the existence of the two parabolic equations (8) and (9) in the governing field equations set, which give rise to the two parabolas in the plane $k_{2i}^* - \omega^*$. Figure 4-(f) is the two-dimensional representation of figure 4-(e) in the plane $k_{2r}^* - \omega^*$. Figure 5 shows the changes that occur in the material band diagrams due to variations in the thermodiffusive coupling in the case $k_1 = 0$. In particular, premultiplying $\boldsymbol{\alpha}$, $\boldsymbol{\beta}$ and ψ in equations (7)-(9) by a scalar coupling factor δ, blue curves of figure 5 represent the case $\delta = 1$, green curves the case $\delta = 0.5$, and red curves the case $\delta = 0$, this last corresponding to the fully uncoupled state. As in figure 4, obtained spectra have been translated along the k_{2r}^* axis using, for each value of δ, a thin and light marker, in order to stress the periodicity of the curves along that axis. Figure 5-(a) is a three-dimensional representation of computed band diagrams for $0 \leq \omega^* \leq 10^3$ showing the behaviour of damping branches. Figure 5-(b) is a zoomed view of the three-dimensional spectra for $-1 \leq k_{2i}^* \leq 1$ depicting the behaviour of propagation branches and figures 5-(c) and 5-(d) are its corresponding two-dimensional representations, respectively in the plane $k_{2r}^* - \omega^*$ and $k_{2i}^* - \omega^*$. As expected, pass bands and band gaps structure of shear waves is not influenced by the value of the coupling factor δ being mechanical shear waves uncoupled from thermal and diffusive fields, while the behaviour of compressional waves results strongly affected by thermodiffusive coupling. In particular, figure 5-(c) shows a broadening of pass bands width as δ increases, with a consequent increase of the mean frequency value of each pass band. On the other hand, figure 5-(d) exhibits a broadening of band gaps width as the coupling factor increases, which is a desirable feature for different frequency sensing and noise isolation applications. Also the mean frequency value of each band gap increases as δ increases. Figure 5-(e) is a three-dimensional representation of the imaginary part of the wave number k_{2i}^* in terms of δ and ω, showing the influence of thermodiffusive coupling upon the behaviour of damping branches. As clearly represented also in figure 5-(f), which is a two-dimensional representation of figure 5-(e) in the plane $k_{2i}^* - \omega^*$ for three selected values of the coupling factor ($\delta = 0$, $\delta = 0.5$, and $\delta = 1$), the external parabolas increase their amplitudes as δ increases, which corresponds, for the same value of frequency ω^*, to a higher spatial attenuation (k_{2i}^* positive) or amplification (k_{2i}^* negative) of the wave as therm-diffusive coupling increases. On the contrary, internal parabolas decrease their amplitudes as δ increases, with a consequent decreasing of the spatial attenuation/amplification of the wave as δ increases for each value of the frequency ω^*. Figure 6 stresses the influence of thermodiffusive coupling upon the behaviour of the first pass band and of the first band gap for compressional waves. In particular, figure 6-(a) depicts the increase of the width of the first pass band A_p^* (light blue curve) and of the fist band gap A_b^* (red curve) as δ increases, while figure 6-(b) shows the increase of the mean frequency value relative to the first pass band $\bar{\omega}_p^*$ (light blue curve) and to the first band gap $\bar{\omega}_b^*$ (red curve) in terms of the coupling factor δ. Both widths and mean frequencies have been adimensionalized with the reference frequency ω_{ref}. Finally, figure 7 refers to spectra obtained for different values of dimensionless wave number $k_1^* = k_1 L$, assumed to have a vanishing imaginary component. Blue curves denote the case $k_1^* = 0$, red curves the case $k_1^* = 0.5\pi$, and green curves the case $k_1^* = \pi$. Figure 7-(a) is a section in $\mathbb{R}^3$ of the hypercurves described in (34) for $-4 \leq k_{2i}^* \leq 4$, showing propagation branches related to the hyperbolic equations (7) in the governing field equations set. Figures 7-(b) and 7-(c) show, respectively, the two-dimensional representations of figure 7-(a) in the planes $k_{2r}^* - \omega^*$ and $k_{2i}^* - \omega^*$. Figure 7-(d) is a zoomed view of obtained spectra in the plane $k_{2r}^* - \omega^*$ for $0 \leq \omega^* \leq 10^3$, illustrating the behaviour of damping branches related to the presence of parabolic equations (8)-(9) in the governing field equations set. It is worth noting that plots in figure 7 are not sufficient in order to investigate the behaviour of a wave propagating inside the thermodiffusive composite materials along directions different from the one that is perpendicular to material layering, for which both k_2 and k_1 vary point by point. They represent obtained complex spectra for a fixed value of wave number k_1, that, when is different from zero, characterizes the plane wave as inhomogeneous, since $\mathbf{n}_r \neq \mathbf{n}_i$ in equation (31).

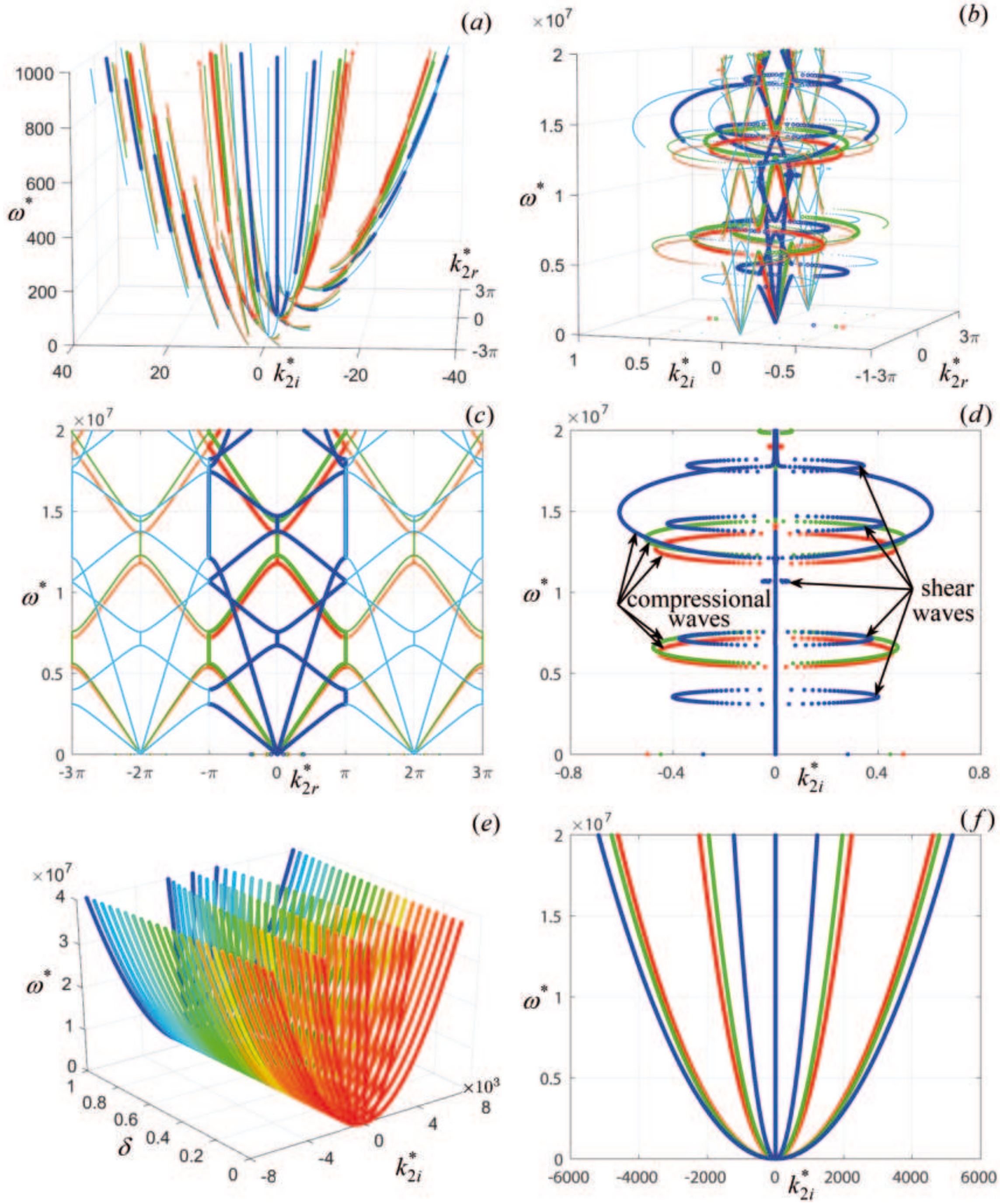

Figure 5: Complex frequency spectrum obtained for $k_1 = 0$ and different values of the coupling factor: $\delta = 0$ (red curves), $\delta = 0.5$ (green curves), and $\delta = 1$ (blue curves). (a) 3D view zoomed for $0 \le \omega^* \le 10^3$; (b) 3D view zoomed for $-1 \le k^*_{2i} \le 1$; (c) plane $k^*_{2r} - \omega^*$ for $-1 \le k^*_{2i} \le 1$; (d) plane $k^*_{2i} - \omega^*$ for $-1 \le k^*_{2i} \le 1$; (e) k^*_{2i} as a function of δ and ω^*; (f) plane $k^*_{2i} - \omega^*$.

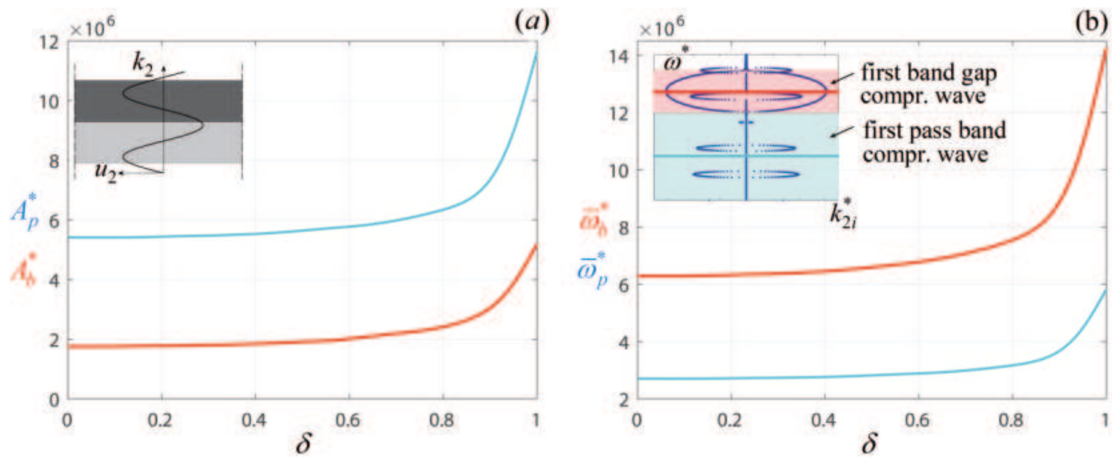

Figure 6: (a) Dimensionless width of the first pass band A_p^* (light blue curve) and of the first band gap A_b^* (red curve) relative to compressional waves vs coupling factor δ; (b) Dimensionless mean frequency of the first pass band $\bar{\omega}_p^*$ (light blue curve) and of the first band gap $\bar{\omega}_b^*$ (red curve) relative to compressional waves vs coupling factor δ.

5 Conclusions

The present work is devoted to investigate the propagation and damping of waves inside composite materials whose phases can be modeled as linear thermodiffusive media. The principal goal is the study and the estimation of the impact that thermal and diffusive effects can have on the propagation of harmonic oscillation in two-dimensional thermodiffusive laminates. Materials frequency band structure and relative dispersion curves are provided in the case of complex-valued wave vectors and real angular frequencies (spatial damping), both for the uncoupled and coupled case and the changes observed in the frequency spectra due to thermodiffusive couplings are discussed in details. In the formulation elastic wave equation is coupled with standard heat conduction and mass diffusion equations, these lasts both of parabolic type and associated to damping phenomena. In order to build material band diagrams, after fixing the value of the wave number in the direction parallel to material layering, a standard eigenvalue problem is solved in terms of the Floquet multiplier by spanning a selected range of frequency, here considered as an independent parameter. Real and imaginary part of the wave number in the direction perpendicular to material layering, which are related, respectively, to the propagation and spatial attenuation (or amplification) of the wave, are then computed from the value of the complex Floquet multiplier. Characteristic polynomial valid for periodic thermodiffusive laminate, whose elementary cell is considered made by an arbitrary number of layers, has been obtained by means of a generalization of the transfer matrix method and by imposing generalized Floquet-Bloch quasiperiodic conditions in the direction perpendicular to material layering. Floquet-Bloch approach allows constructing a band diagram for an entire periodic medium by analyzing the dynamics of only a single unit cell. Illustrative examples are provided, applying the developed general method to study the propagation and damping of harmonic mechanical, thermal, and diffusive oscillations to bi-phase isotropic thermodiffusive laminates of interest for SOFCs applications. Vulnerability to damage of such devices can increase because of typical high operating temperature and intensive ions flows and an accurate prediction of their performances reveals to be of fundamental importance in order to not undermine their efficiency. By varying the value of coupling terms in the governing field equations set, a broadening of band gaps widths associated to compressional waves has been obtained as thermodiffusive coupling increases, which is a desirable feature in different isolation and sensing applications. Furthermore, also the mean frequency value of pass bands and band gaps relative to mechanical compressional waves increases as the coupling increases. Homogeneous and inhomogeneous waves have been investigated, depending on whether the normals to planes having constant phase are parallel to normals to planes with constant amplitude or not.

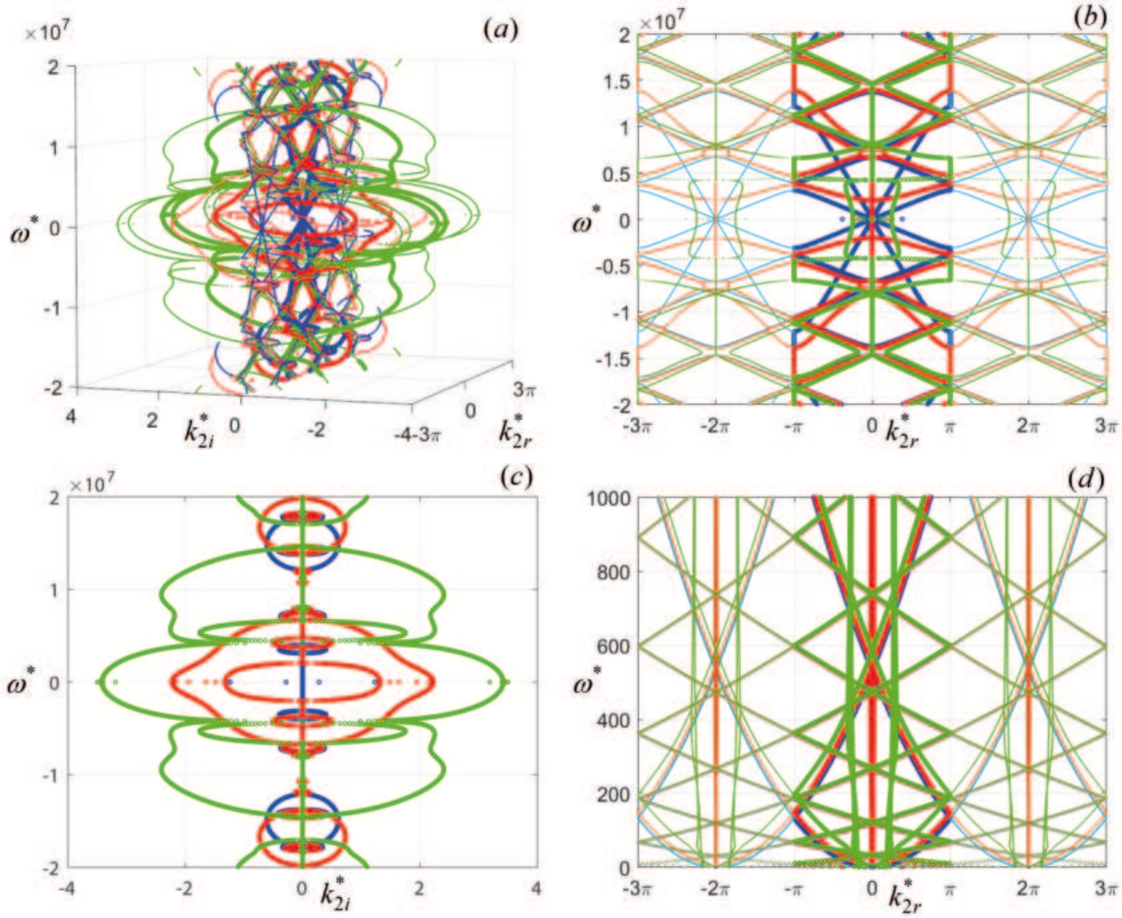

Figure 7: Complex material spectra obtained for $k_1^* = 0$ (blue curves), $k_1^* = 0.5\,pi$ (red curves), $k_1^* = \pi$ (green curves). (a) 3D view for $-4 \le k_{2i}^* \le 4$; (b) plane $k_{2r}^* - \omega^*$ for $-4 \le k_{2i}^* \le 4$; (c) plane $k_{2i}^* - \omega^*$ for $-4 \le k_{2i}^* \le 4$; (d) plane $k_{2r}^* - \omega^*$ for $0 \le \omega^* \le 10^3$.

Appendix A. Matrix exponential determination for a single layer of the composite laminate

General formal solution of the system (16) can be expressed in the form

$$\mathbf{r} = a\boldsymbol{\gamma}\exp\left[-\varsigma x_2\right], \tag{42}$$

where a is a constant, $\boldsymbol{\gamma}$ is the eigenvector corresponding to the eigenvalue ς, solution of the following associate eigenvalues problem

$$\mathbf{H}(\varsigma)\boldsymbol{\gamma} = \mathbf{0}, \tag{43}$$

with $\mathbf{H}(\varsigma) = \mathbf{N} - \varsigma\mathbf{M}$. The existence of non-trivial solutions of the algebraic system (43) requires the vanishing of the determinant of the matrix $\mathbf{H}$. This yields an eight-degree polynomial characteristic equation having the form

$$\mathcal{Q}(\varsigma) = \mathrm{Det}\left(\mathbf{H}(\varsigma)\right) = \mathcal{Q}_8\varsigma^8 + \mathcal{Q}_6\varsigma^6 + \mathcal{Q}_4\varsigma^4 + \mathcal{Q}_2\varsigma^2 + \mathcal{Q}_0 = 0. \tag{44}$$

The solution of equation (44) gives the complete eigenvalues spectrum. Assuming that this equation admits eight different solutions, and then that all eigenvalues are distinct, for each one of them one can determine the associate eigenvector $\boldsymbol{\gamma}^{(i)}$ with $i = 1, ..., 8$. In this way, one obtains a complete set of eigenfunctions, which represents a basis of the solutions space, and the general solution can be written as a linear combination of these eigenfunctions

$$\mathbf{r} = \boldsymbol{\Gamma}\,\mathbf{E}\,\mathbf{a}, \tag{45}$$

where $\boldsymbol{\Gamma} = \left(\boldsymbol{\gamma}^{(1)}\,\boldsymbol{\gamma}^{(2)}\,\boldsymbol{\gamma}^{(3)}\,\boldsymbol{\gamma}^{(4)}\,\boldsymbol{\gamma}^{(5)}\,\boldsymbol{\gamma}^{(6)}\,\boldsymbol{\gamma}^{(7)}\,\boldsymbol{\gamma}^{(8)}\right)$ is the eigenvectors matrix with eigenvectors arranged by column,
$\mathbf{a} = (a_1\,a_2\,a_3\,a_4\,a_5\,a_6\,a_7\,a_8)^T$ is a constant vector, and $\mathbf{E}$ is a diagonal matrix of the form

$$\begin{aligned} \mathbf{E} \;&=\; \mathrm{diag}\left[\exp\left[-\varsigma^{(1)}x_2\right], \exp\left[-\varsigma^{(2)}x_2\right], \exp\left[-\varsigma^{(3)}x_2\right], \exp\left[-\varsigma^{(4)}x_2\right], \exp\left[-\varsigma^{(5)}x_2\right],\right. \\ &\left.\exp\left[-\varsigma^{(6)}x_2\right], \exp\left[-\varsigma^{(7)}x_2\right], \exp\left[-\varsigma^{(8)}x_2\right]\right]. \end{aligned} \tag{46}$$

Matrix $\mathbf{E}$ is diagonalizable when algebraic multiplicity of the eigenvalues equals their geometric multiplicity, otherwise $\mathbf{E}$ assumes the form of a Jordan block diagonal matrix. Note that assuming the form (45) for the solution of the system (16) implies that all the eigenvalues γ_j are distinct. If some eigenvalues are identical, the exponential matrix assumes a more complicated form including terms depending by x_2^n, where n is the degree of degeneracy of the system (Arfken and Weber, 2005). Matrices $\boldsymbol{\Gamma}$ and $\mathbf{E}$, together with constitutive relation (38) and the fluxes definitions (39) and (40) are used to derive an explicit expression for the generalized amplitude vector $\mathbf{z} = (\mathbf{w}\,\mathbf{t})^T$, which components are given by

$$\mathbf{z}(x_2) = \left(\tilde{u}_1(x_2)\;\tilde{u}_2(x_2)\;\tilde{\theta}(x_2)\;\tilde{\eta}(x_2)\;\tilde{\sigma}_{21}(x_2)\;\tilde{\sigma}_{22}(x_2)\;\tilde{q}_2(x_2)\;\tilde{j}_2(x_2)\right)^T, \tag{47}$$

and then for the generalized solution $\mathbf{y} = (\mathbf{v}\;\mathbf{s})^T = \mathbf{z}\exp\left[i\left(\mathbf{k}\cdot\mathbf{x} - \omega t\right)\right]$. Vectors $\mathbf{z}$ and $\mathbf{y}$ assume respectively the form

$$\mathbf{z} = \boldsymbol{\Omega}\,\mathbf{E}\,\mathbf{a}, \quad \mathbf{y} = \boldsymbol{\Omega}\,\mathbf{E}\,\mathbf{a}\exp\left[i\left(\mathbf{k}\cdot\mathbf{x} - \omega t\right)\right], \tag{48}$$

where the explicit expressions for the lines of the 8×8 matrix $\boldsymbol{\Omega}$ are

$$\begin{gathered} \Omega_{1j} = \gamma_j^{(5)}, \quad \Omega_{2j} = \gamma_j^{(6)}, \quad \Omega_{3j} = \gamma_j^{(7)}, \quad \Omega_{4j} = \gamma_j^{(8)}, \\ \Omega_{5j} = G(\gamma_j^{(1)} + ik_1\gamma_j^{(6)} + ik_2\gamma_j^{(5)}), \\ \Omega_{6j} = \frac{2G(1-\nu)}{1-2\nu}\gamma_j^{(2)} + \frac{2ik_1G\nu}{1-2\nu}\gamma_j^{(5)} + \frac{2ik_2G(1-\nu)}{1-2\nu}\gamma_j^{(6)} - \alpha\gamma_j^{(7)} - \beta\gamma_j^{(8)}, \\ \Omega_{7j} = -K(\gamma_j^{(3)} + ik_2\gamma_j^{(7)}), \quad \Omega_{8j} = -D(\gamma_j^{(4)} + ik_2\gamma_j^{(8)}), \quad \text{with} \;\; j = 1, \ldots, 8. \end{gathered} \tag{49}$$

The second of (48) represents the formal generalized solution of the problem valid for each m^{th} layer composing the periodic cell of the laminate. Applying the transfer matrix method, equations (48) could be exploited for studying the propagation and the attenuation of oscillations induced by periodic boundary conditions on the whole multi-layered material.

Appendix B. Recursive algorithm to determine the invariants of a characteristic polynomial

Eigenvalues of problem (29) are the roots of a characteristic polynomial $\mathcal{P}(\lambda)$ of the 8^th degree, which can be written in the form

$$\mathcal{P}(\lambda) = C_0 + C_1\lambda + C_2\lambda^2 + C_3\lambda^3 + C_4\lambda^4 + C_5\lambda^5 + C_6\lambda^6 + C_7\lambda^7 + C_8\lambda^8 \tag{50}$$

The present Section describes a recursive method, called the Faddeev-LeVerrier algorithm (Horst et al., 1935), in order to compute the invariants of characteristic polynomial (50). Coefficients C_k of (50) are recursively computed by means of the following formulas

$$\mathbf{M}_0 = \mathbf{0}, \quad C_8 = 1 \ \text{ at step } k = 0, \tag{51a}$$

$$\mathbf{M}_k = \mathbf{A}\mathbf{M}_{k-1} + C_{n-k+1}\mathbf{I}, \quad C_{n-k} = -\frac{1}{k}\mathrm{tr}\left[\mathbf{A}\mathbf{M}_k\right] \ \text{ at step } k = 1, ..., 8 \tag{51b}$$

with matrix $\mathbf{A} = \mathbf{T}_{(1,n)}$ and $\mathbf{M}_k$ auxiliary matrices. Applying equations (51) one finally has

$$C_7 = -\mathrm{tr}\left[\mathbf{A}\right], \tag{52a}$$

$$C_6 = -\frac{1}{2}\mathrm{tr}\left[\mathbf{A}^2\right] + \frac{1}{2}\left(\mathrm{tr}\left[\mathbf{A}\right]\right)^2, \tag{52b}$$

$$C_5 = -\frac{1}{3}\mathrm{tr}\left[\mathbf{A}^3\right] + \frac{1}{2}\mathrm{tr}\left[\mathbf{A}^2\right]\mathrm{tr}\left[\mathbf{A}\right] - \frac{1}{6}\left(\mathrm{tr}\left[\mathbf{A}\right]\right)^3, \tag{52c}$$

$$C_4 = -\frac{1}{4}\mathrm{tr}\left[\mathbf{A}^4\right] + \frac{1}{3}\mathrm{tr}\left[\mathbf{A}\right]\mathrm{tr}\left[\mathbf{A}^3\right] + \frac{1}{8}\left(\mathrm{tr}\left[\mathbf{A}^2\right]\right)^2 - \frac{1}{4}\mathrm{tr}\left[\mathbf{A}^2\right]\left(\mathrm{tr}\left[\mathbf{A}\right]\right)^2 + \frac{1}{24}\left(\mathrm{tr}\left[\mathbf{A}\right]\right)^4, \tag{52d}$$

$$\begin{aligned} C_3 = &-\frac{1}{5}\mathrm{tr}\left[\mathbf{A}^5\right] + \frac{1}{4}\mathrm{tr}\left[\mathbf{A}\right]\mathrm{tr}\left[\mathbf{A}^4\right] + \frac{1}{6}\mathrm{tr}\left[\mathbf{A}^2\right]\mathrm{tr}\left[\mathbf{A}^3\right] - \frac{1}{6}\left(\mathrm{tr}\left[\mathbf{A}\right]\right)^2\mathrm{tr}\left[\mathbf{A}^3\right] \\ &- \frac{1}{8}\left(\mathrm{tr}\left[\mathbf{A}^2\right]\right)^2\mathrm{tr}\left[\mathbf{A}\right] + \frac{1}{12}\left(\mathrm{tr}\left[\mathbf{A}\right]\right)^3\mathrm{tr}\left[\mathbf{A}^2\right] - \frac{1}{120}\left(\mathrm{tr}\left[\mathbf{A}\right]\right)^5, \end{aligned} \tag{52e}$$

$$\begin{aligned} C_2 = &-\frac{1}{6}\mathrm{tr}\left[\mathbf{A}^6\right] + \frac{1}{5}\mathrm{tr}\left[\mathbf{A}\right]\mathrm{tr}\left[\mathbf{A}^5\right] + \frac{1}{8}\mathrm{tr}\left[\mathbf{A}^2\right]\mathrm{tr}\left[\mathbf{A}^4\right] - \frac{1}{8}\mathrm{tr}\left[\mathbf{A}^4\right]\left(\mathrm{tr}\left[\mathbf{A}\right]\right)^2 \\ &+ \frac{1}{18}\left(\mathrm{tr}\left[\mathbf{A}^3\right]\right)^2 - \frac{1}{6}\mathrm{tr}\left[\mathbf{A}\right]\mathrm{tr}\left[\mathbf{A}^2\right]\mathrm{tr}\left[\mathbf{A}^3\right] + \frac{1}{18}\mathrm{tr}\left[\mathbf{A}^3\right]\left(\mathrm{tr}\left[\mathbf{A}\right]\right)^3 - \frac{1}{48}\left(\mathrm{tr}\left[\mathbf{A}^2\right]\right)^3 \\ &+ \frac{1}{16}\left(\mathrm{tr}\left[\mathbf{A}^2\right]\right)^2\left(\mathrm{tr}\left[\mathbf{A}\right]\right)^2 - \frac{1}{48}\left(\mathrm{tr}\left[\mathbf{A}\right]\right)^4\mathrm{tr}\left[\mathbf{A}^2\right] + \frac{1}{720}\left(\mathrm{tr}\left[\mathbf{A}\right]\right)^6, \end{aligned} \tag{52f}$$

$$\begin{aligned} C_1 = &-\frac{1}{7}\mathrm{tr}\left[\mathbf{A}^7\right] + \frac{1}{6}\mathrm{tr}\left[\mathbf{A}\right]\mathrm{tr}\left[\mathbf{A}^6\right] + \frac{1}{10}\mathrm{tr}\left[\mathbf{A}^2\right]\mathrm{tr}\left[\mathbf{A}^5\right] - \frac{1}{10}\left(\mathrm{tr}\left[\mathbf{A}\right]\right)^2\mathrm{tr}\left[\mathbf{A}^5\right] \\ &+ \frac{1}{12}\mathrm{tr}\left[\mathbf{A}^3\right]\mathrm{tr}\left[\mathbf{A}^4\right] - \frac{1}{8}\mathrm{tr}\left[\mathbf{A}\right]\mathrm{tr}\left[\mathbf{A}^2\right]\mathrm{tr}\left[\mathbf{A}^4\right] + \frac{1}{24}\left(\mathrm{tr}\left[\mathbf{A}\right]\right)^3\mathrm{tr}\left[\mathbf{A}^4\right] \\ &- \frac{1}{18}\mathrm{tr}\left[\mathbf{A}\right]\left(\mathrm{tr}\left[\mathbf{A}^3\right]\right)^2 - \frac{1}{24}\left(\mathrm{tr}\left[\mathbf{A}^2\right]\right)^2\mathrm{tr}\left[\mathbf{A}^3\right] + \frac{1}{12}\left(\mathrm{tr}\left[\mathbf{A}\right]\right)^2\mathrm{tr}\left[\mathbf{A}^2\right]\mathrm{tr}\left[\mathbf{A}^3\right] \\ &- \frac{1}{72}\left(\mathrm{tr}\left[\mathbf{A}\right]\right)^4\mathrm{tr}\left[\mathbf{A}^3\right] + \frac{1}{48}\mathrm{tr}\left[\mathbf{A}\right]\left(\mathrm{tr}\left[\mathbf{A}^2\right]\right)^3 - \frac{1}{48}\left(\mathrm{tr}\left[\mathbf{A}\right]\right)^3\left(\mathrm{tr}\left[\mathbf{A}^2\right]\right)^2 \\ &+ \frac{1}{240}\left(\mathrm{tr}\left[\mathbf{A}\right]\right)^5\mathrm{tr}\left[\mathbf{A}^2\right] - \frac{1}{5040}\left(\mathrm{tr}\left[\mathbf{A}\right]\right)^7, \end{aligned} \tag{52g}$$

$$\begin{aligned} C_0 = &-\frac{1}{8}\mathrm{tr}\left[\mathbf{A}^8\right] + \frac{1}{7}\mathrm{tr}\left[\mathbf{A}\right]\mathrm{tr}\left[\mathbf{A}^7\right] + \frac{1}{12}\mathrm{tr}\left[\mathbf{A}^2\right]\mathrm{tr}\left[\mathbf{A}^6\right] - \frac{1}{12}\left(\mathrm{tr}\left[\mathbf{A}\right]\right)^2\mathrm{tr}\left[\mathbf{A}^6\right] \\ &+ \frac{1}{15}\mathrm{tr}\left[\mathbf{A}^3\right]\mathrm{tr}\left[\mathbf{A}^5\right] - \frac{1}{10}\mathrm{tr}\left[\mathbf{A}\right]\mathrm{tr}\left[\mathbf{A}^2\right]\mathrm{tr}\left[\mathbf{A}^5\right] + \frac{1}{30}\left(\mathrm{tr}\left[\mathbf{A}\right]\right)^3\mathrm{tr}\left[\mathbf{A}^5\right] \\ &- \frac{1}{12}\mathrm{tr}\left[\mathbf{A}\right]\mathrm{tr}\left[\mathbf{A}^3\right]\mathrm{tr}\left[\mathbf{A}^4\right] - \frac{1}{32}\left(\mathrm{tr}\left[\mathbf{A}^2\right]\right)^2\mathrm{tr}\left[\mathbf{A}^4\right] + \frac{1}{16}\left(\mathrm{tr}\left[\mathbf{A}\right]\right)^2\mathrm{tr}\left[\mathbf{A}^2\right]\mathrm{tr}\left[\mathbf{A}^4\right] \\ &- \frac{1}{96}\left(\mathrm{tr}\left[\mathbf{A}\right]\right)^4\mathrm{tr}\left[\mathbf{A}^4\right] - \frac{1}{36}\mathrm{tr}\left[\mathbf{A}^2\right]\left(\mathrm{tr}\left[\mathbf{A}^3\right]\right)^2 + \frac{1}{36}\left(\mathrm{tr}\left[\mathbf{A}\right]\right)^2\left(\mathrm{tr}\left[\mathbf{A}^3\right]\right)^2 \\ &+ \frac{1}{24}\mathrm{tr}\left[\mathbf{A}\right]\left(\mathrm{tr}\left[\mathbf{A}^2\right]\right)^2\mathrm{tr}\left[\mathbf{A}^3\right] - \frac{1}{36}\left(\mathrm{tr}\left[\mathbf{A}\right]\right)^3\mathrm{tr}\left[\mathbf{A}^2\right]\mathrm{tr}\left[\mathbf{A}^3\right] + \frac{1}{360}\left(\mathrm{tr}\left[\mathbf{A}\right]\right)^5\mathrm{tr}\left[\mathbf{A}^3\right] \\ &+ \frac{1}{384}\left(\mathrm{tr}\left[\mathbf{A}^2\right]\right)^4 - \frac{1}{96}\left(\mathrm{tr}\left[\mathbf{A}\right]\right)^2\left(\mathrm{tr}\left[\mathbf{A}^2\right]\right)^3 + \frac{1}{192}\left(\mathrm{tr}\left[\mathbf{A}^2\right]\right)^2\left(\mathrm{tr}\left[\mathbf{A}\right]\right)^4 \end{aligned}$$

$$-\frac{1}{1440}\left(\mathrm{tr}\left[\,\mathbf{A}\,\right]\right)^6\mathrm{tr}\left[\,\mathbf{A}^2\,\right]+\frac{1}{32}\left(\mathrm{tr}\left[\,\mathbf{A}^4\,\right]\right)^2+\frac{1}{40320}\left(\mathrm{tr}\left[\,\mathbf{A}\,\right]\right)^8 \tag{52h}$$

Since for a characteristic n^{th}-degree characteristic polynomial, coefficient $C_0 = (-1)^n \mathrm{Det}(\mathbf{A})$,the Faddeev-LeVerrier algorithm can also be exploited as a procedure to compute the determinant of a square matrix $\mathbf{A}$, which is usually a computationally expensive process. When matrix $\mathbf{A}$ is symplectic, as in the standard eigenvalue problem (29), the characteristic polynomial is palindromic (Bronski and Rapti, 2005), meaning that $\mathcal{P}(\lambda) = \sum_{j=0}^{2N} C_j \lambda^j$ with $C_{2N-j} = C_j$ and $N = 4$. It can be proved from equations (52) that $C_8 = C_0 = 1$, $C_7 = C_1$, $C_6 = C_2$ e $C_5 = C_3$ and the 8^{th}-degree polynomial $\mathcal{P}(\lambda)$ written as

$$\mathcal{P}(\lambda) = 1 + C_1\lambda + C_2\lambda^2 + C_3\lambda^3 + C_4\lambda^4 + C_3\lambda^5 + C_2\lambda^6 + C_1\lambda^7 + \lambda^8 \tag{53}$$

results to be equivalent to the 4^{th}-degree polynomial $\tilde{\mathcal{P}}(z)$

$$\tilde{\mathcal{P}}(z) = z^4 + C_1 z^3 + (C_2 - 4)\,z^2 + (C_3 - 3C_1)\,z + (C_4 - 2C_2 + 2)\,, \tag{54}$$

under conformal map $z = \lambda + \frac{1}{\lambda}$. Roots of polynomial (54) can be analytically expressed.

Appendix C. Transfer matrix as power series of wave number k_1

When spatial damping (complex-valued wave vector $\mathbf{k}$ and real-valued angular frequency omega) has to be investigated, transfer matrix $\mathbf{T}_m$ relative to the m^{th} layer of the composite material introduced in equation (25), could be expressed as a power series of the wave number k_1. Denoting again with $\mathbf{F} = \mathbf{M}^{-1}\mathbf{N}\ell_m$, matrix exponential $\exp[\mathbf{F}]$, defined as in (60), is a function of the wave numbers k_1 and k_2, and of the angular frequency ω, namely $\exp[\mathbf{F}] = f(k_1, k_2, \omega)$. Based on expressions (15) and (17), matrix $\mathbf{F}$ can be decomposed as

$$\mathbf{F} = \mathbf{H}_0 + k_1\mathbf{H}_1 + k_1^2\mathbf{H}_2, \tag{55}$$

where $\mathbf{H}_0$ collects terms that do not depend upon k_1, $\mathbf{H}_1$ collects terms that linearly depend upon k_1, and $\mathbf{H}_2$ collects terms that depend upon k_1^2. Matrix exponential $\exp[\mathbf{F}]$ can therefore be expressed as

$$\exp[\mathbf{F}] = \sum_{n=0}^{+\infty}\frac{1}{n!}\left(\mathbf{H}_0 + k_1\mathbf{H}_1 + k_1^2\mathbf{H}_2\right)^n \tag{56}$$

Based upon the expression of the n^{th} power of trinomial $\left(\mathbf{H}_0 + k_1\mathbf{H}_1 + k_1^2\mathbf{H}_2\right)$, namely

$$\begin{aligned}\left(\mathbf{H}_0 + k_1\mathbf{H}_1 + k_1^2\mathbf{H}_2\right)^n &= \sum_{r_1+r_2+r_3=n} n!\prod_{i=1}^{3}\frac{\left(\mathbf{F}_{i-1}k_1^{i-1}\right)^{r_i}}{r_i!} = \\ &= \sum_{j=0}^{n}\sum_{s=0}^{n-j}\frac{n!}{j!s!(n-j-s)!}\mathbf{H}_0^{n-j-s}\left(k_1\mathbf{H}_1\right)^s\left(k_1^2\mathbf{H}_2\right)^j\,,\end{aligned} \tag{57}$$

equation (25) assumes the form

$$\begin{aligned}\mathbf{y}_m^+ &= \begin{pmatrix}\mathbf{0} & \mathbf{I}\\ \mathbf{R} & i\mathbf{R}k_2+\mathbf{S}\end{pmatrix}\left[\sum_{n=0}^{+\infty}\sum_{j=0}^{n}\sum_{s=0}^{n-j}\frac{1}{j!s!(n-j-s)!}\mathbf{H}_0^{n-j-s}\left(k_1\mathbf{H}_1\right)^s\left(k_1^2\mathbf{H}_2\right)^j\right] \\ &\quad \begin{pmatrix}\mathbf{0} & \mathbf{I}\\ \mathbf{R} & i\mathbf{R}k_2+\mathbf{S}\end{pmatrix}^{-1}\exp\left[ik_2\ell_m\right]\mathbf{y}_m^-,\end{aligned} \tag{58}$$

Consequently, transfer matrix $\mathbf{T}_m$ referred to the m^{th} layer of the laminate, shows a polynomial dependence upon wave number k_1 in the form

$$\mathbf{T}_m = \sum_{n=0}^{+\infty}\sum_{j=0}^{n}\sum_{s=0}^{n-j}\frac{k_1^{s+2j}}{j!s!(n-j-s)!}\begin{pmatrix}\mathbf{0} & \mathbf{I}\\ \mathbf{R} & i\mathbf{R}k_2+\mathbf{S}\end{pmatrix}\mathbf{H}_0^{n-j-s}\mathbf{H}_1^s\mathbf{H}_2^j$$

$$\begin{pmatrix} \mathbf{0} & \mathbf{I} \\ \mathbf{R} & i\mathbf{R}k_2 + \mathbf{S} \end{pmatrix}^{-1} \exp\left[ik_2\ell_m\right] \tag{59}$$

Transfer matrix of the entire unit cell $\mathbf{T}_{(1,n)} = \prod_{i=0}^{n-1} \mathbf{T}_{n-i}$, therefore, results to be expressed as a power series of k_1 and a suitable truncation of it can be employed in order to investigated wave propagation in the $\mathbf{e}_1$ direction.

Appendix D. Transfer matrix as power series of angular frequency ω

In order to investigate temporal damping for the material of interest (complex-valued angular frequency ω and real-valued wave numbers k_1 and k_2), transfer matrix $\mathbf{T}_m$ introduced in equation (25) relative to the m^{th} material layer, could be expressed as a power series of the angular frequency ω. Referring to equation (25), and denoting with $\mathbf{F} = \mathbf{M}^{-1}\mathbf{N}\ell_m$, matrix exponential $\exp\left[\mathbf{F}\right]$, defined as

$$\exp\left[\mathbf{F}\right] = \sum_{n=0}^{+\infty} \frac{1}{n!}\mathbf{F}^n, \tag{60}$$

is a function of wave numbers k_1 and k_2 and angular frequency ω, namely $\exp\left[\mathbf{F}\right] = f\left(k_1, k_2, \omega\right)$. Based on expressions (15) and (17), matrix $\mathbf{F}$ can be decomposed as

$$\mathbf{F} = \mathbf{G}_0 + \omega\mathbf{G}_1 + \omega^2\mathbf{G}_2, \tag{61}$$

collecting in $\mathbf{G}_0$ terms that do not depend upon ω, in $\mathbf{G}_1$ terms that linearly depend upon $omega$, and in $\mathbf{G}_2$ terms that depend upon ω^2. Doing this, matrix exponential $\exp\left[\mathbf{F}\right]$ results to be expressed as

$$\exp\left[\mathbf{F}\right] = \sum_{n=0}^{+\infty} \frac{1}{n!}\left(\mathbf{G}_0 + \omega\mathbf{G}_1 + \omega^2\mathbf{G}_2\right)^n \tag{62}$$

Since the n^{th} power of trinomial $\left(\mathbf{G}_0 + \omega\mathbf{G}_1 + \omega^2\mathbf{G}_2\right)$ can be written as

$$\begin{aligned} \left(\mathbf{G}_0 + \omega\mathbf{G}_1 + \omega^2\mathbf{G}_2\right)^n &= \sum_{r_1+r_2+r_3=n} n! \prod_{i=1}^{3} \frac{\left(\mathbf{G}_{i-1}\omega^{i-1}\right)^{r_i}}{r_i!} = \\ &= \sum_{j=0}^{n}\sum_{s=0}^{n-j} \frac{n!}{j!s!(n-j-s)!}\mathbf{G}_0^{n-j-s}\left(\omega\mathbf{G}_1\right)^s\left(\omega^2\mathbf{G}_2\right)^j \end{aligned} \tag{63}$$

one obtains that equation (25) is expressed in the form

$$\begin{aligned} \mathbf{y}_m^+ &= \begin{pmatrix} \mathbf{0} & \mathbf{I} \\ \mathbf{R} & i\mathbf{R}k_2 + \mathbf{S} \end{pmatrix} \left[\sum_{n=0}^{+\infty}\sum_{j=0}^{n}\sum_{s=0}^{n-j} \frac{1}{j!s!(n-j-s)!}\mathbf{G}_0^{n-j-s}\left(\omega\mathbf{G}_1\right)^s\left(\omega^2\mathbf{G}_2\right)^j\right] \\ &\quad \begin{pmatrix} \mathbf{0} & \mathbf{I} \\ \mathbf{R} & i\mathbf{R}k_2 + \mathbf{S} \end{pmatrix}^{-1} \exp\left[ik_2\ell_m\right]\mathbf{y}_m^-, \end{aligned} \tag{64}$$

Transfer matrix $\mathbf{T}_m$ relative to the m^{th} layer of the laminate, therefore, results to show a polynomial dependence upon angular frequency ω, namely

$$\begin{aligned} \mathbf{T}_m &= \sum_{n=0}^{+\infty}\sum_{j=0}^{n}\sum_{s=0}^{n-j} \frac{\omega^{s+2j}}{j!s!(n-j-s)!} \begin{pmatrix} \mathbf{0} & \mathbf{I} \\ \mathbf{R} & i\mathbf{R}k_2 + \mathbf{S} \end{pmatrix} \mathbf{G}_0^{n-j-s}\,\mathbf{G}_1^s\,\mathbf{G}_2^j \\ &\quad \begin{pmatrix} \mathbf{0} & \mathbf{I} \\ \mathbf{R} & i\mathbf{R}k_2 + \mathbf{S} \end{pmatrix}^{-1} \exp\left[ik_2\ell_m\right]. \end{aligned} \tag{65}$$

From equation (65), transfer matrix of the entire unit cell $\mathbf{T}_{(1,n)} = \prod_{i=0}^{n-1} \mathbf{T}_{n-i}$, results to be expressed as a power series of ω and its truncation to a proper order can be exploited in order to investigated temporal damping.

Acknowledgments

The authors acknowledge the financial support from National Group of Mathematical Physics (GNFM-INdAM). MP would like to acknowledge financial support from the Italian Ministry of Education, University and Research (MIUR) to the research project of relevant national interest (PRIN 2017) "XFAST-SIMS: Extra-fast and accurate simulation of complex structural systems" (CUP: D68D19001260001).

References

Anandakumar, G., Li, N., Verma, A., Singh, P., Kim, J.-H., 2010. Thermal stress and probability of failure analyses of functionally graded solid oxide fuel cells. J. Power Sources 195, 6659–6670.

Arfken, G. B., Weber, H. J., 2005. Mathematical methods for physicists, 5th edition. Elsevier Academic Press, San Diego.

Atkinson, A., Sun, B., 2007. Residual stress and thermal cycling of planar solid oxide fuel cells. Mater. Sci. Tech. 23, 1135–1143.

Bacca, M., Bigoni, D., Dal Corso, F., Veber, D., 2013a. Mindlin second-gradient elastic properties from dilute two-phase Cauchy-elastic composites. Part I: closed form expression for the effective higher-order constitutive tensor. Int. J. Solids Struct. 50, 4010–4019.

Bacca, M., Bigoni, D., Dal Corso, F., Veber, D., 2013b. Mindlin second-gradient elastic properties from dilute two-phase Cauchy-elastic composites. Part II: higher-order constitutive properties and application cases. Int. J. Solids Struct. 50, 4020–4029.

Bacigalupo, A., Gambarotta, L., 2014. Second-gradient homogenized model for wave propagation in heterogeneous periodic media. Int. J. Solids Struct. 51, 1052–1065.

Bacigalupo, A., Morini, L., Piccolroaz, A., 2014. Effective elastic properties of planar SOFCs: a non-local dynamic homogenization approach. Int. J. Hydrogen Energy 39, 15017–15030.

Bacigalupo, A., Morini, L., Piccolroaz, A., 2016a. Multiscale asymptotic homogenization analysis of thermo-diffusive composite materials. Int. J. Solids Struct. 85-86, 15–33.

Bacigalupo, A., Morini, L., Piccolroaz, A., 2016b. Overall thermomechanical properties of layered materials for energy devices applications. Comp. Struct. 157, 366–385.

Bakhvalov, N. S., Panasenko, G. P., 1984. Homogenization: averaging processes in periodic media. Kluwer Academic Publishers, Dordrecht-Boston-London.

Bigoni, D., Drugan, W. J., 2007. Analytical derivation of Cosserat moduli via homogenization of heterogeneous elastic materials. ASME J. Appl. Mech. 74, 741–753.

Bloch, F., 1929. Über die quantenmechanik der elektronen in kristallgittern. Zeitschrift für physik 52 (7-8), 555–600.

Bove, R., Ubertini, S., 2008. Modeling solid oxide fuel cells: methods, procedures and techniques. Springer, Netherlands.

Brandon, N. P., Brett, D. J., 2006. Engineering porous materials for fuel cell applications. Phil. Trans. R. Soc. A 364, 147–159.

Brillouin, L., 1953. Wave propagation in periodic structures: electric filters and crystal lattices.

Bronski, J. C., Rapti, Z., 2005. Modulational instability for nonlinear schrödinger equations with a periodic potential. Dynamics of Partial Differential Equations 2 (4), 335–355.

Carcione, J., 2007. Wave fields in real media: Wave propagation in anisotropic, anelastic, porous and electromagnetic media. Elsevier.

Carta, G., Brun, M., 2015. Bloch–floquet waves in flexural systems with continuous and discrete elements. Mechanics of Materials 87, 11–26.

Carta, G., Brun, M., Movchan, A. B., Boiko, T., 2016. Transmission and localisation in ordered and randomly-perturbed structured flexural systems. International Journal of Engineering Science 98, 126–152.

Caviglia, G., Morro, A., 1992. Inhomogeneous waves in solids and fluids. Vol. 7. World Scientific.

Colpan, C. O., Dincer, I., Hamdullahpur, F., 2008. A review on macro-level modeling of planar solid oxide fuel cells. International Journal of Energy Research 32 (4), 336–355.

De Bellis, M. L., Addessi, D., 2011. A Cosserat based multi-scale model for masonry structures. Int. J. Multiscale Comput. Eng. 9, 543–563.

Delette, G., Laurencin, J., Usseglio-Viretta, F., Villanova, J., Bleuet, P., Lay-Grindler, E. e. a., 2013. Thermoelastic properties of SOFC/SOEC electrode materials determined from threedimensional microstructural reconstructions. Int. J. Hydrogen Energy 38, 12379–12391.

Dev, B., Walter, M. E., Arkenberg, G. B., Swartz, S. L., 2014. Mechanical and thermal characterization of a ceramic/glass composite seal for solid oxide fuel cells. J. Power Sources 245, 958–966.

Ellis, B. L., Kaitlin, T., Nazar, L. F., 2012. New composite materials for lithium-ion batteries. Electrochimica Acta 84, 145–154.

Fantoni, F., Bacigalupo, A., 2020. Wave propagation modeling in periodic elasto-thermo-diffusive materials via multifield asymptotic homogenization. International Journal of Solids and Structures 196–197, 99–128.

Fantoni, F., Bacigalupo, A., Paggi, M., 2017. Multi-field asymptotic homogenization of thermo-piezoelectric materials with periodic microstructure. International Journal of Solids and Structures 120, 31–56.

Fantoni, F., Bacigalupo, A., Paggi, M., 2018. Design of thermo-piezoelectric microstructured bending actuators via multi-field asymptotic homogenization. International Journal of Mechanical Sciences 146, 319–336.

Fantoni, F., Bacigalupo, A., Paggi, M., Reinoso, J., 2019. A phase field approach for damage propagation in periodic microstructured materials. International Journal of Fracture, 1–24.

Faulkner, M., Hong, D., 1985. Free vibrations of a mono-coupled periodic system. Journal of Sound and Vibration 99 (1), 29–42.

Floquet, G., 1883. Sur les équations différentielles linéaires à coefficients périodiques 12, 47–88.

Forest, S., 2002. Homogenization methods and the mechanics of generalised continua–part 2. Theor. Applied Mech. 28, 113–143.

Forest, S., Trinh, D. K., 2011. Generalised continua and nonhomogeneous boundary conditions in homogenisation. Z. Angew. Math. Mech. 91, 90–109.

Gupta, G. S., 1970. Natural flexural waves and the normal modes of periodically-supported beams and plates. Journal of Sound and Vibration 13 (1), 89–101.

Hajimolana, S. A., Hussain, M. A., Wan Daud, W. M. A., Soroush, M., Shamiri, A., 2011. Mathematical modeling of solid oxide fuel cells: a review. Renew. Sustain Energy Rev. 15, 1893–1917.

Hasanov, R., Smirnova, A., Gulgazli, A., Kazimov, M., Volkov, A., Quliyeva, V., Vasylyev, O., Sadykov, V., 2011. Modeling design and analysis of multi-layer solid oxide fuel cells. International journal of hydrogen energy 36 (2), 1671–1682.

Hawwa, M. H., Nayfeh, A. H., 1995. The general problem of thermoelastic waves in anisotropic periodically laminated composites. Comp. Eng. 5, 1499–1517.

Hennig, D., Tsironis, G. P., 1999. Wave transmission in nonlinear lattices. Physics Reports 307 (5-6), 333–432.

Horst, P., et al., 1935. A method for determining the coefficients of a characteristic equation. The Annals of Mathematical Statistics 6 (2), 83–84.

Johnson, J., Qu, J., 2008. Effective modulus and thermal expansion of Ni-YSZ porous cermets. J. Power Sources 181, 85–92.

Kakac, S., Pramuanjaroenkij, A., Zhou, X. Y., 2007. A review of numerical modeling of solid oxide fuel cells. International journal of hydrogen energy 32 (7), 761–786.

Kamotski, I. V., Smyshlyaev, V. P., 2019. Bandgaps in two-dimensional high-contrast periodic elastic beam lattice materials. Journal of the Mechanics and Physics of Solids 123, 292–304.

Kim, J. H., Liu, W. K., Lee, C., 2009. Multi-scale solid oxide fuel cell materials modeling. Computational Mechanics 44 (5), 683–703.

Kuebler, J., Vogt, U. F., Haberstock, D., Sfeir, J., Mai, A., Hocker, T., Roos, M., Harnisch, U., 2010. Simulation and validation of thermo-mechanical stresses in planar sofcs. Fuel Cells 10 (6), 1066–1073.

Langley, R., 1993. A note on the force boundary conditions for two-dimensional periodic structures with corner freedoms. Journal of Sound and Vibration 167, 377–381.

Lew, T., Scarpa, F., Worden, K., 2004. Homogenisation metamodelling of perforated plates. Strain 40 (3), 103–112.

Lord, H. M., Shulman, Y., 1967. A generalized dynamical theory of thermoelasticity. J. Mech. Phys. Solids 15, 299–309.

Mead, D., 1973. A general theory of harmonic wave propagation in linear periodic systems with multiple coupling. Journal of Sound and Vibration 27 (2), 235–260.

Molla, T. T., Kwok, K., Frandsen, H. L., 2016. Efficient modeling of metallic interconnects for thermo-mechanical simulation of sofc stacks: homogenized behaviors and effect of contact. International Journal of Hydrogen Energy 41 (15), 6433–6444.

Monchiet, V., Auffray, N., Yvonnet, J., 2020. Strain-gradient homogenization: a bridge between the asymptotic expansion and quadratic boundary condition methods. Mechanics of Materials 143, 103309.

Muramatsu, M., Terada, K., Kawada, T., Yashiro, K., Takahashi, K., Takase, S., 2015. Characterization of time-varying macroscopic electro-chemo-mechanical behavior of sofc subjected to ni-sintering in cermet microstructures. Computational Mechanics 56 (4), 653–676.

Nakajo, A., Kuebler, J., Faes, A., Vogt, U. F., Schindler, H. J., Chiang, L. K. e. a., 2012. Compilation of mechanical properties for the structural analysis of solid oxide fuel cell stacks. Constitutive materials of anode-supported cells. Ceram. Int. 38, 3907–3927.

Nowacki, W., 1974a. Dynamical problems of thermodiffusion in solids. I. Bull. Polish Acad. Sci. Tech. Sci. 22, 55–64.

Nowacki, W., 1974b. Dynamical problems of thermodiffusion in solids. II. Bull. Polish Acad. Sci. Tech. Sci. 22, 205–211.

Nowacki, W., 1974c. Dynamical problems of thermodiffusion in solids. III. Bull. Polish Acad. Sci. Tech. Sci. 22, 257–266.

Paggi, M., Corrado, M., Rodriguez, M. A., 2013. A multi-physics and multi-scale numerical approach to microcracking and power-loss in photovoltaic modules. Comp. Struct. 95, 630–638.

Richardson, G., Denuault, G., Please, C. P., 2012. Multiscale modelling and analysis of lithium-ion battery charge and discharge. J. Eng. Mat. 72, 41–72.

Romeo, F., Luongo, A., 2002. Invariant representation of propagation properties for bi-coupled periodic structures. Journal of sound and vibration 257 (5), 869–886.

Salvadori, A., Bosco, E., Grazioli, D., 2014. A computational homogenization approach for Li-ion battery cells: Part1–formulation. J. Mech. Phys. Solids 65, 114–137.

Scarpa, F., Adhikari, S., Phani, A. S., 2009. Effective elastic mechanical properties of single layer graphene sheets. Nanotechnology 20 (6), 065709.

Sherief, H. H., Hamza, F. A., Saleh, H. A., 2004. The theory of generalized thermoelastic diffusion. Int. J. Eng. Sci. 42, 591–608.

Smyshlyaev, V. P., Cherednichenko, K. D., 2000. On rigorous derivation of strain gradient effects in the overall behaviour of periodic heterogeneous media. J. Mech. Phys. Solids 48, 1325–1357.

Wang, Z., Poh, L. H., Dirrenberger, J., Zhu, Y., Forest, S., 2017. Isogeometric shape optimization of smoothed petal auxetic structures via computational periodic homogenization. Computer Methods in Applied Mechanics and Engineering 323, 250–271.

Xiao, Y., Wen, J., Yu, D., Wen, X., 2013. Flexural wave propagation in beams with periodically attached vibration absorbers: band-gap behavior and band formation mechanisms. Journal of Sound and Vibration 332 (4), 867–893.

Yvonnet, J., Auffray, N., Monchiet, V., 2020. Computational second-order homogenization of materials with effective anisotropic strain-gradient behavior. International Journal of Solids and Structures 191, 434–448.

Zhu, W. Z., Deevi, S. C., 2003. A review on the status of anode materials for solid oxide fuel cells. Mat. Sci. Eng. A 362, 228–239.